ZnO nanostructures for dye sensitized solar cells

By

Ahad Hussain Javed

Reg # 00000204633

Session 2017-19

Supervised by

Dr. Nadia Shahzad

A Thesis Submitted to the US-Pakistan Center for Advanced Studies in Energy in partial fulfillment of the requirements for the degree of

MASTER of SCIENCE

in

ENERGY SYSTEMS ENGINEERING

US-Pakistan Center for Advanced Studies in Energy (USPCAS-E)

National University of Sciences and Technology (NUST)

H-12, Islamabad 44000, Pakistan

August 2021

THESIS ACCEPTANCE CERTIFICATE

Certified that final copy of MS thesis written by **Mr. Ahad Hussain Javed**, (Registration No. 000204633), of U.S.-Pakistan center for Advanced Studies in Energy has been vetted by undersigned, found complete in all respects as per NUST Statues/Regulations, is within the similarity indices limit and is accepted as partial fulfillment for the award of MS degree. It is further certified that necessary amendments as pointed out by GEC members of the scholar have also been incorporated in the said thesis.

Signature: _____

Name of Supervisor Dr. Nadia Shahzad

Date: _____

Signature (HoD): _____

Date: _____

Signature (Dean/Principal): _____

Date: _____

CERTIFICATE

This is to certify that work in this thesis has been carried out by **Mr. Ahad Hussain Javed** and completed under my supervision in Solar Energy Laboratory, US-Pakistan Center for Advanced Studies in Energy (USPCAS-E), National University of Sciences and Technology, H-12, Islamabad, Pakistan.

Supervisor:

_____

Dr. Nadia Shahzad
USPCAS-E,
NUST H-12, Islamabad

Co-Supervisor:

_____

Dr. M Abdullah Khan
Department of Env. Sciences,
QAU, Islamabad

GEC member # 1:

_____

Dr. Naseem Iqbal
USPCAS-E,
NUST H-12, Islamabad

GEC member # 2:

_____

Dr. Muhammad Hassan
USPCAS-E,
NUST H-12, Islamabad

HoD- ESE:

_____

Dr. Rabia Liaquat
USPCAS-E,
NUST H-12, Islamabad

Principal/ Dean:

_____

Dr. Adeel Waqas
USPCAS-E,
NUST H-12, Islamabad

Dedication

*To **Almighty Allah**, for his daily blessings, make all my work possible.*

To my Parents, for their endless love, support and encouragement

*To my younger sister **Maria Qubtia,** who have always motivated me to pace towards my goals.*

To my dearest homeland, Pakistan

Acknowledgments

First and foremost, I would like to thank **Almighty ALLAH** who is the creator of everything and all respects for His **Prophet Muhammad** (PBUH, On Whom Be ALLAH'S Blessings and Salutations). In fact, without His blessings, this difficult and diligence task would have been impossible.

I would like to express my hearty thanks and respect to my supervisor **Dr. Nadia Shahzad**, for her support and guidance. I am extremely thankful and indebted to her for sharing expertise, valuable guidance and encouragement extended to me. I appreciate her act of providing me various options of joining research projects with different research groups. She was very kind and cool mind towards me throughout this research. I am once again really grateful to her.

I would like to pay my gratitude to my co-supervisor **Dr. Abdullah Khan** for being available whenever I need him. His support and guidance make me able to achieve this task. His kind guidance always proven a lime light throughout this journey.

I take this opportunity to express gratitude to all of the Department faculty members for their help and support. I also thank my parents and siblings for the encouragement, support, love and attention.

I also place on record, my sense of gratitude to one and all, who directly or indirectly, have lent their hand in this venture.

I pay my regards to my GEC members for their utmost support and guidance throughout this research project. I am also grateful to USPCAS-E, for allowing me to use their lab facilities.

Regards,

Ahad Hussain Javed

Abstract

Development of cost effective and easily scalable energy systems for harvesting renewable solar energy is attractive proposal for future. This work presents facile synthesis of ZnO nanostructures with different morphologies simply providing different solvating conditions in a hydrothermal process, for their subsequent use in dye sensitized solar cell (DSSC) device. ZnO nanoprisms were obtained in aqueous solution where addition of methanol/ethanol resulted in formation of hollow nanoprims while methanol in alkaline solution yield ZnO nanorice morphology. The obtained nanostructures were characterized for structural, morphological, elemental, optical and surface area analysis. Then devices were fabricated using the grown nanostructure and tested their response under 1 sun conditions for dye sensitized solar cells with N719 dye loading. Among the different nanostructure morphologies, ZnO nonorice showed superior performance reaching the maximum conversion efficiency. We attribute this to the large surface area, better conductivity, and enhanced dye adsorption of nanorice in comparison to the other synthesized ZnO nanostructures.

Keywords: *ZnO, Hexagonal nanoprsim, Nanorice, Hydrothermal, Dye sensitized solar cells*

Table of Contents

List of Figures

List of Tables

Publications

Journal Paper

1. ***Effect of ZnO nanostructures on the performance of dye sensitized solar cells (Journal: Solar Energy) (Under Review)***
2. ***Highly Fluorescent Hemicyanine and Dicyanoisophorone Dyes: Synthesis and Applications in DSSCs (Journal: Spectrochimica Acta Part A: Molecular and Biomolecular Spectroscopy) (Under Review)***

Conference Paper

3. ***Synthesis and Characterization of Cobalt redox couple based liquid electrolytes and quasi-solid electrolytes for applications in Dye-Sensitized Solar Cells (International Conference on Sustainable Energy Technologies) (Accepted)***

Other Publications

4. ***Designing of Homemade Soiling Station to Explore Soiling Loss Effects on PV Modules (Journal: Solar Energy) (Accepted)***
5. ***Nitrogen-rich mesoporous carbon for high temperature reversible CO2 capture (*Journal of CO2 Utilization) *(Published)***
6. ***Synthesis of bi-metallic Co-Ni/ZnO Nanoprisms (ZnO-NPr) for hydrogen rich syngas production via partial oxidation of methane (Journal: Hydrogen energy) (Ready for submission)***

List of Abbreviations

DSSC	Dye Sensitized solar cell
EQE	External Quantum efficiency
XRD	X-Ray Diffractometery
SEM	Scanning electron microscopy
FTO	Fluorine Doped tin oxide
ZnO	Zinc Oxide
TiO_2	Titinia
^oC	Degree Celsius
PMMA	Polymethylmethacrylate
PDMS	Polydimethylsiloxane
HOMO	Higher occupied molecular orbital
LUMO	Lower unoccupied molecular orbital
CVD	Chemical vapor deposition
PVD	Physical vapor deposition
ED	Electrochemical deposition
WE	Working electrode
CE	Counter electrode
RE	Reference electrode
BET	Brunner-Emmett teller

mM	Milli molar
cm^2	Centimeter square
mA	Milli Amperes
w/m^2	Watts Per Meter Square
UV	Ultra Violet
Voc	Open Circuit voltage
Jsc	Short Circuit Current Density

Chapter 1

Introduction

1.1. Background

Industrial and economic development give rise to the energy demand. In the result of increased energy demand use of fossil fuels increased to meet with requirements of new industrialized world which causes adverse effects on our environment and give rise to its prices. Industries being a major emitter of CO_2 in the result fossil fuels usage is the most challenging problem [1,2]

A new energy economy is emerging as a response to such issues and as a means of promoting a more sustainable future [3]. Among all the renewable and clean energy sources such as wind, solar, geothermal, biomass, hydropower, tidal and biomass, solar is the most prominent kind of energy and abundantly available. Even a little conversion could help us to fulfil our needs of energy and address the problem of rising price and demand of energy. In 2018, primary energy consumption increased by 2.9 percent, nearly double of the 10-year's average which was 1.5 percent. Carbon emissions increased by 2.0 percent, while the annual average price of fuel oil increased by 2.0 percent to $71.31/barrel, from $54.19/barrel in 2017. On average, 1.4 million barrels of oil are produced per year.

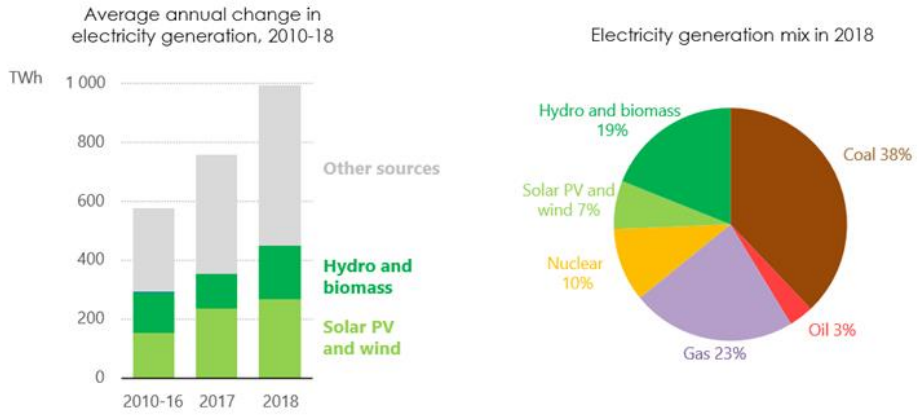

Fig. 1.1: Average annual change in electricity generation 2010-2018 [5].

In 2018, the cost of all commercial renewable and clean energy technologies fell. The average cost of CSP (concentrated solar power) has decreased by 26%, biofuel by 14%, onshore wind and solar photovoltaic (PV) both by 13%, hydropower by 12%,

and geothermal and offshore wind both by 1%. The cost of onshore wind and solar photovoltaic power is cheaper than that of fossil fuels. [6].

In recent decades, this steady drop and low-cost decarbonization have aroused researchers' attention. As a result, significant efforts are being made to boost the usage of renewable and sustainable energy sources near in future to address the rising energy demand and fossil fuel exhaustion.

1.2. Renewable Energy Technologies.

The key renewable technologies are listed below.

- Wind Energy
- Bioenergy
- Hydropower
- Geothermal
- Tidal energy
- Solar Energy

From 2018 to 2023, the renewable energy contribution is predicted to increase by 1/5th each year to meet global energy demand. Renewables are predicted to provide 30% of worldwide demand in 2023, which was 24% in 2017, with solar photovoltaic leading the way, followed by wind, hydro, and biofuels. Hydropower has a 16 percent share, followed by wind at 6%, solar at 4%, and biofuel at 3%. Similarly, heating is predicted to increase by 10% to 12%, and transportation by 10% to 12%.[7].

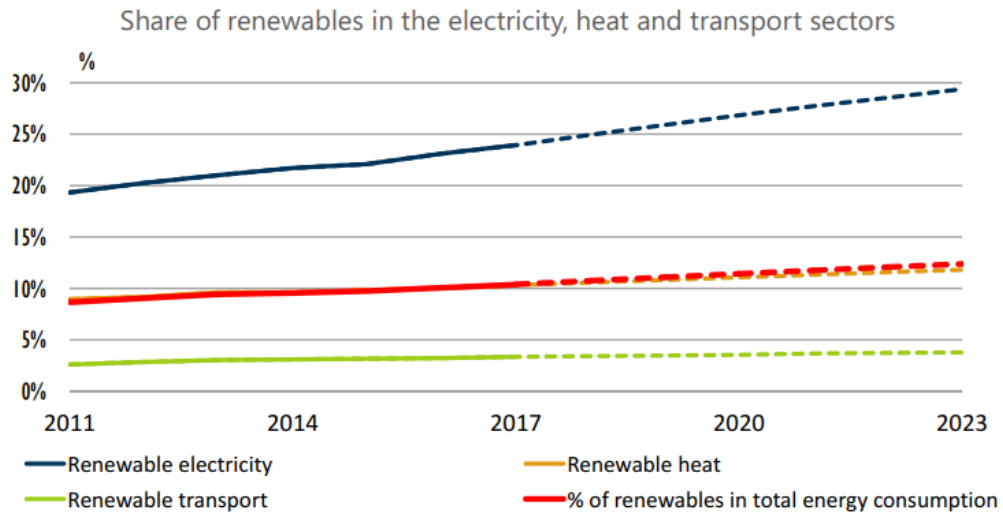

Fig. 1.2: Renewable Energy resources share [7]

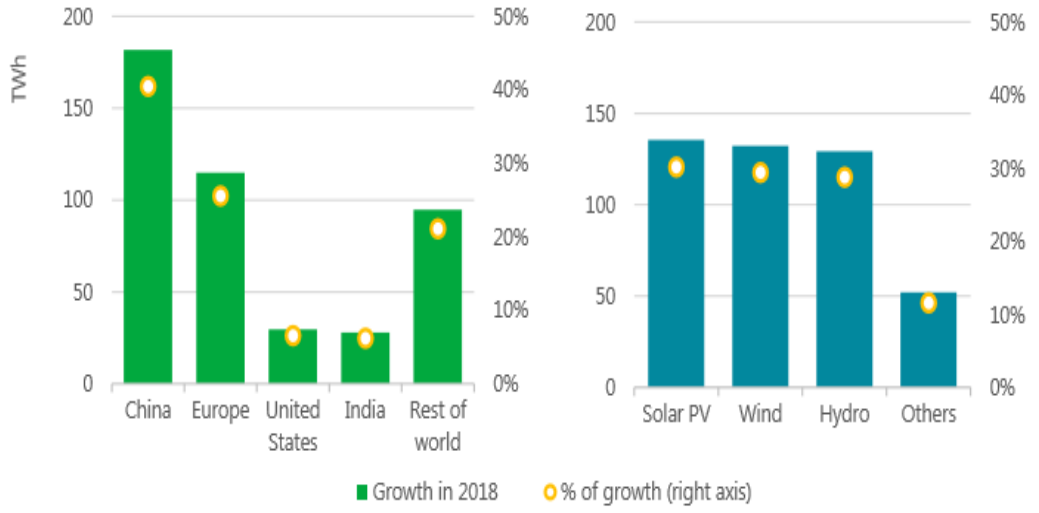

Fig. 1.3: Regional and technological growth in renewable electricity generating [5].

1.2.1. Wind Energy

Wind energy is a type of solar energy produced by the sun's uneven heating of the earth's surface. During the day, the air over the land is hotter than the air above the ocean, thus hot air began to expand and rise, causing cool air rush to take place of expanded air, causing wind [8]. Only around 2% of solar energy is transferred to wind, and around 35% of that energy is wasted within 1000 metres. The total amount of wind power available is around 1.26×10^{9}MW, which is enough to supply the world's entire energy need. The kinetic energy of the wind is converted into mechanical energy, which is then used to generate electricity by a wind turbine. Modern wind turbines typically have three blades and can generate power up to several megawatts at reasonably high wind speeds [9].

1.2.2. Bioenergy

Bioenergy can pay a constructive role in achieving the sustainable development [10]. Bioenergy is derived from biomass. Biomass is an organic matter which is directly or indirectly produced by using CO_2 and water from environment in presence of sunlight by photosynthesis. Solar energy is stored in the form of chemical energy and can be converted into electricity, heat and transport fuels. Biomass may include wood from plantation forest, residue from forest, crop & timber industry, vegetable oil, animal fats and organic waste from industry, animal husbandry and human settlements [11,12].

There are many routes to convert raw biomass into useful products. Several conversion techniques exist or being development to produce the useful energy from biomass. For the purpose of electricity.

In a coal-fired power plant, co-firing is the most cost-effective option. In both power and combined heat and power generation (CHP) plants, dedicated biomass combustion units are in commercial operation. Anaerobic digestion is also being used in electricity generation sector and proved a best suited option. Further improvement will leads to more cleaner, reliable system linked to electricity, heat and higher quality fuel generation [13].

1.2.3. Hydropower

Hydropower comes from the moving water. It converts the kinetic and mechanical energy of water to generate electricity. It appears to be a form of solar energy, as the sun drives the hydrologic cycle, which facilitates rain. Atmospheric water reaches the earth's surface as rain in the hydrologic cycle. Some of the water evaporates, but the majority of it percolates into the soil and become surface runoff. Rain and melting snow eventually reach ponds, lakes, reservoirs, and oceans, where they can be used to generate electricity. [14]. With more than 150 countries producing hydroelectric electricity, hydropower is the world's largest renewable resource and plays an important role in many regions of the globe. Norway, Bhutan, Paraguay and several African countries are among the ten countries of the world that get almost all of their commercial electricity from hydro. Around 700GW of hydro capacity is expected to be operational globally, generating 2600TWh/year (about 19% of global energy production) [15].

1.2.4. Geothermal

Geothermal energy, also known as Earth heat, is a clean and sustainable resource. Geothermal energy is the most adaptable renewable energy source, have been utilised for thousands of years washing, bathing, cooking, and health. The use of hot water directly has a long history and continues to grow, as new applications emerge. Late in 2013, twenty-four countries were using geothermal energy to generate electricity, and 78 countries were using geothermal energy for heating. The total installed geothermal capacity in the globe was 10.7GWe, and it is continually growing every day [16]. Some geothermal energy uses rely on the earth's temperatures near the surface, while others

necessitate drilling kilometres below the ground. The three primary applications of geothermal energy are as follows [17]:

- **Direct Use:** which make use of hot water from nearby springs or reservoirs
- **Power generation:** Power plants need a high temperature steam and water ranging from 300 to700 degree Fahrenheit. So, the Geothermal power stations are constructed where the reservoirs are within one or two miles from the surface.
- **Geothermal heat pumps:** used to control temperature of buildings, employ stable ground or water temperatures near the earth's surface.

1.2.5. Tidal Energy

Tidal Energy is a new and developing technology that is not yet economically feasible and is currently in the research and development stage. Tidal energy is an endless source of energy that can be classified as renewable. It is advantageous because it is less subject to climate change than the other sources, which are all susceptible to unpredictable climate variations [18]. It is estimated that the worldwide theoretically harvestable tidal energy supply from locations near the coast is 1 terawatt (TW). Tidal current technologies have a greater promise than tidal range technologies. In 2012, the total tidal range deployment was roughly 514 MW. Up to 2020, tidal current deployment forecasts are in the 200 MW range. Energy can be generated at any time of day or night. Furthermore, weather conditions have little impact on tidal range. For power generation, tidal generation offers a variety of alternatives [19].

- One-way power generation at ebb tide.
- One-way power generation at flood tide.
- Two-way power generation.

1.2.6. Solar Energy

Solar energy is one of the most well-known sources of renewable energy, and it may be used in three different ways: electric, thermal, and chemical. Despite the quantity of solar energy, humans only utilize a small portion of this vast resource. Solar energy represents for only 0.015 percent of total worldwide electricity output, while solar heat contributes for only 0.3 percent of worldwide space and water heating. Biomass production by natural processes, as well as its combustion and gasification, are the most common uses of solar energy. Solar energy is mostly used to produce hydrogen

using the photocatalysis technology, which accounts for around 11% of human energy needs [20].

1.3. Solar Energy Potential in Pakistan

Renewable energy development and effective use is growing in Pakistan. Pakistan is one of those countries where the sun shines almost all the year and has a significant solar power producing potential. Average solar radiations throughout the country remains 136.05W/m^2 to 287.36W/m^2. More of the period of year sun shines for 10 hours a day that could result in 45-83MW power per month from just 100m^2 area. From March to October, the intensity of solar radiation stays favourable across the country. From February to October in Sindh, from March to October in Baluchistan, from April to September in the NWFP, Northern regions, and Kashmir region, and from March to October in Punjab, the radiation intensity remains greater than 200W/m^2. Throughout the year, solar energy has a promising potential in most portions of southern Punjab, Sindh, and Baluchistan. The annual sun direct normal irradiance in the southern region of Pakistan is above 5kWh/m^2/day, which is ideal for photovoltaic technologies. [21].

1.4. Harvesting Techniques:

Solar Energy can be harvested by three techniques [20].

1. Solar Fuel
2. Solar Thermal
3. Electricity

1.4.1 Solar Fuel

Solar energy into hydrogen generation via splitting of water is supposed to be an aspirant fuel in future as it is a clean, green and sustainable approach to elevate the global energy and alleviate environmental problems. Although numerous technologies have been established and are using for hydrogen production, only a few can be considered eco-friendly. The fundamental process of natural photosynthesis for sunlight to chemical energy conversion which further constitutes the bio building blocks of all living organisms provides the best baseline idea for hydrogen production in an intermediate process. Since, natural systems are unamendable and the hydrogen

is produced in sporadic concentrations, research progresses focus on imitating photosynthesis artificially.

Researchers have been striving to assemble an "artificial leaf" that efficiently captures, convert and stores solar energy as high-energy chemical fuel. Artificial photosynthesis is believed to be a promising technology not only in terms of efficient, eco-friendly and sustainable energy setup but also the formation of viable energy-laden fuels through water splitting and CO2 sequestration.

1.4.2 Solar Thermal

Solar energy is converted into thermal energy for usage in homes and businesses, such as drying, heating, and cooling. solar flat plate collectors are used for such purposes where high temperature is not required, while for high temperature applications concentrated systems are used. To minimize serious damage to the environment and living beings, solar thermal energy is also employed for saline removal and wastewater treatment. Solar thermal refrigerators, which are separated into sorption refrigerators and solar thermal mechanical refrigerators, are becoming increasingly popular in both agriculture and the commercial sector [20-23].

1.4.3 Electricity

Electricity generation is further divided into two categories [22].

- PV Technologies
- Solar Thermal Power generation

1.4.3.1 Solar Thermal Power Generation

Electricity is generated using concentrated solar power technology. High magnification mirrors are used to concentrate solar energy at a point where water is converted into steam. Similarly, Fresnel mirrors, solar dish and power towers used to concentrate solar energy onto a receiving tube, a single point and a reflector above the ground level respectively for high temperature applications. Power used the array of thousands of reflecting mirrors [22,23].

1.4.3.2 PV Technologies

PV technologies involving the semiconductor to convert sunlight into electricity. Solar photons have the ability to drive an electron across a semiconductor's bandgap,

resulting in an electron-hole pair at p-n junction interface. Generated electron moves in one direction while hole in other which in a result creates a potential difference equal to band gap [20].

1.5. Research Motivation and Objectives

One of the major reasons which limit the performance is the inefficient electron transport due to recombination of photo-generated electrons. Improving photoanode properties can overcome this problem. For a better understanding, further research is required, how differently exposed facets act to improve the DSSC's overall performance. This project is an attempt to understand basic processes happening at ZnO surface.

The main objective is to untangle electrons accumulation and conduction behavior and dynamics in relation to a particular facet of a nanostructure. The other important aspect is to develop an economical and facile material process for the synthesis of ZnO, to improve dye-sensitized solar cells overall performance with a distinct electrical conduction.

1.6. Thesis outline

1. Chapter 2 describes the literature review related to DSSCs and photoanode materials (i.e TiO_2 and ZnO) as well as ZnO synthesis and its applications for DSSCs.
2. Chapter 3 covers the detailed overview of experimental and characterizations techniques being used extensively for photoanode materials.
3. Chapter 4 deals with experimental work carried out in lab including the cell fabrication.
4. Chapter 5 describes the experimentation results carried out for photoanode material and assembled cells.
5. Chapter 6 includes the conclusion and recommendations.

Summary

This chapter describes the motivation behind the selection of this topic. In this chapter the need of renewable energy and importance of each technology is extensively discussed specially, solar and how we can harness this potential energy source. Both the global and Pakistan solar potential has been discussed. This chapter also includes the objectives of this research. The last section is comprising of outlines of this thesis that how it would proceed.

References

[1] *Global Warming-The Complete Briefing 4th edition*. 2009.

[2] "Statistics CO_2 emissions from fuel combustion," 2016.

[3] U. S. News, W. Report, W. Post, and T. Guardian, *Praise for Plan B*. 2007.

[4] "BP Statistical Review of World Energy Statistical Review of World," 2019.

[5] U. S. Energy, "International Energy Outlook 2017 Overview," 2017.

[6] International Renewable Energy Agency and Irena, *RENEWABLE POWER GENERATION COSTS IN 2018*. 2018.

[7] International Energy Agency, "Renewables 2018," 2018.

[8] E. F. Wind, "Wind Energy -- Energy from Moving Air."

[9] W. Tong, "Fundamentals of Wind Energy," vol. 44, 2009.

[10] U. Energy, "Bioenergy-Annual Report 2017," 2017.

[11] J. Ness and B. Moghtaderi, "Biomass and Bioenergy," 2016.

[12] U. Rasool and S. Hemalatha, "A review on bioenergy and biofuels : sources and their production," 2016.

[13] W. E. Council, "World Energy Resources: Bioenergy," pp. 1–24, 2013.

[14] US Department of the Interior bureau of reclamation, "Hydroelectric Power."

[15] S. Algburi, "Hydroelectric Power," 2017.

[16] H. Saibi, S. Finsterle, L. Berkeley, R. Bertani, and J. Nishijima, "Geothermal Energy," 2013.

[17] U. S. Department of Energy, "Geothermal Energy - Energy from the Earth ' s Core," 2020.

[18] J. K. Seelam, "Tidal Energy : A Review TIDAL ENERGY : A REVIEW,"2016.

[19] I. R. E. Agency and Irena, "TIDAL ENERGY," 2014.

[20] G. W. Crabtree, N. S. Lewis, G. W. Crabtree, and N. S. Lewis, "Solar energy conversion," vol. 37, 2018.

[21] S. Adnan, N. Drought, M. Centre, A. H. Khan, S. Haider, and R. Mahmood,

"Solar energy potential in Pakistan Solar energy potential in Pakistan," 2012.

[22] E. Kabir, P. Kumar, S. Kumar, A. A. Adelodun, and K. Kim, "Solar energy : Potential and future prospects," vol. 82, pp. 894–900, 2018.

[23] N. Kannan and D. Vakeesan, "Solar energy for future world : - A review," vol. 62, pp. 1092–1105, 2016.

Chapter 2

Literature Review

2.1 Dye sensitized solar cell (DSSC)

Since Gratzel et al. proposed a titanium dioxide (TiO_2) photoanode-based dye sensitized solar cell (DSSC) in 1991, the field has gotten a lot of interest of researchers. [1]. DSSC is a promising low-cost solar energy conversion device that is simple to manufacture, requiring only 1/10 ~ 1/15 of the total cost of traditional Si-based solar cells. T.Yano et al. reported the improved overall efficiency of 14% after two decades of invention [2].

2.1.1 Principles of Dye-Sensitized Solar Cells

For many years an extensive study carried out on solar energy conversion, however, DSSCs have become a popular renewable energy source in recent years. Michael Gratzel and Brian O'Regan first presented this novel PV technology in 1991. It needs a relatively simple manufacturing process allowing a low-cost and moderately efficient solar cells [3]. Furthermore, dye sensitized solar cells do not follow the typical silicon-based solar cells principle; instead, distinct components of the cell assume the light absorption and charge transfer roles. The semiconductor's principal role is to promote charge transmission, while the dye is employed to absorb photons. The advantages of DSSCs over conventional p-n junction solar cells are numerous. Here are some of the benefits of DSSCs in comparison with silicon based solar cells. Low-cost production as well as material flexibility, including substrates, and the ability to operate over a wide temperature range are all advantages [4]. The dye's electrons are stimulated by incident sunlight. The energized electron travels to the electron collecting glass substrate after being injected into the metal oxide's conduction band. The electron travels from the anode to the counter electrode via the connected circuit, accomplishing valuable work. The oxidized dye is regenerated by the electrolyte's reducing agent. The oxidized species of the electrolyte is reduced to its original condition once the electron has travelled through the load and been collected at the counter electrode. The circuit is now complete, and the cyclic flow of electrons from the anode to the cathode that was discussed earlier continues [20,21]. The open circuit

voltage is difference between redox potential and fermi level of metal oxide. There are eight different basic process occurring in DSSCs which were identified by *Jose et al.* [4].

- Light absorption by dye molecules
- Rate constant for returning an excited dye to its ground state (k1)
- Electron injection from excited dye to semiconductor conduction band-rate constant
- Exciton diffusion through dye material (Dext) (k2)
- Rate constant for electron back transport to oxidized electrolyte species (k3)
    - Transport of electron which is supported by diffusion process across the conduction band (De);
    - Due to interactions between phonon and electrons there is some loss of energy known as phonon relaxation
- Rate constant for electron recombination with oxidized dye molecules (k4)

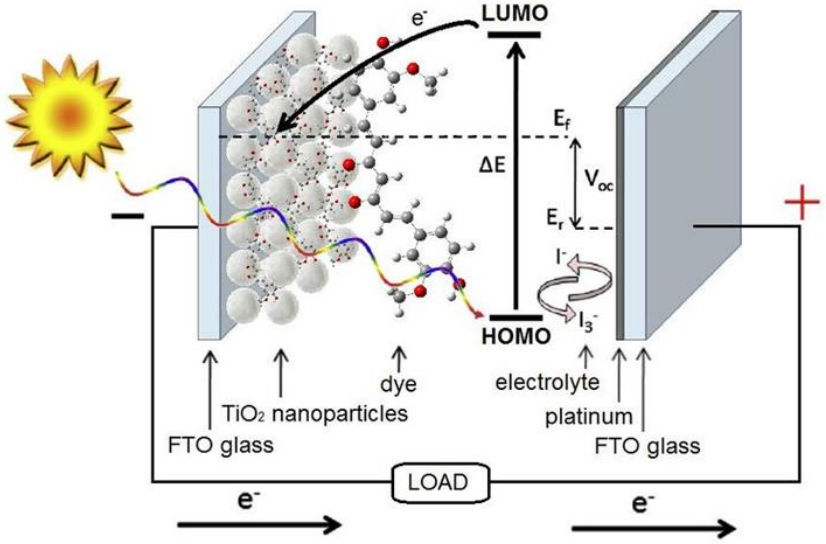

Fig. 2.1: Schematic illustration of DSSCs operation [4]

2.1.2 Components of DSSC

2.1.2.1 Dyes/Sensitizers

The dye molecules are chemically adsorbed on metal oxide photoanode. The electron moves from HOMO to LOMO after absorbing photons from incident light, where it is injected into metal oxide. In the DSSC, dye molecules perform photon-induced electron production and injection for light. The quantity of dye molecules accessible

for light harvesting in DSSCs is governed by the amount of dye loaded on the metal oxide photoanode, which means that the number of dye molecules available for light harvesting in DSSCs is determined by the amount of dye loaded on the metal oxide photoanode (to be discussed in section 2.1.2.4) [7,8].

2.1.2.2 Electrolyte in DSSCs

Electrolyte is a DSSC component that is responsible for the regeneration of oxidized dye as well as electron transport. A redox pair (i.e., I^-/I^{-3}), appropriate organic solvents (in order to ensure that solutes dissolve properly and are evenly dispersed), and additives are commonly found in liquid electrolytes (to improve stability or viscosity). For faster dye regeneration and improved electron transportation performance, a number of redox couples have been investigated [9]. Other than (I^-/I^{-3}) [10] redox couples, such as pseudo halogen-based redox (SCN_2/SCN^-) [11] and cobalt (III/II)-based redox complexes [12] have been examined in this regard. Because of its low cost and ease of synthesis, the (I^-/I^{-3}) redox pair is still the most widely utilized and investigated. As a result, it is frequently used in DSSC photoanode and dye performance testing as a standard electrolyte.

2.1.2.3 Counter electrodes

This is the component of the DSSC construction that completes the cell and electrical circuit. The surface of the counter electrode that receives electrons to reduce the oxidized redox mediator back to its non-oxidized state [13–15]. For this purpose, Pt based counter electrode is used, the major drawback of Pt based counter electrode is its high cost. Various new counter electrodes, such as metal-based, carbon-based, inorganic compound-based, and organic conductive polymer-based counter electrodes, have been created to reduce costs [16,17].

2.1.2.4 The nanostructured metal oxide photoanode

TiO_2 was the photoanode material in the first DSSC reported by Grätzel in 1991, and the photoanode layer is generally 5-20 m thick of nanomaterials [3]. This layer has a large internal surface area that can be accessed by dye molecules for dye loading in order to harvest solar energy. This component is crucial in the dye adsorption and electron transport processes. To date, much work has gone into photoanode research in order to improve the overall performance of DSSCs. The first is to improve the mesoporous photoanode's light trapping capabilities [18], second, surface changes to

improve dye loading ability and reduce recombination [19,20]. However, despite numerous efforts, the recombination concerns with the TiO_2 photoanode have yet to be resolved. The drawbacks of employing TiO_2 nanoparticle-based mesoporous photoanodes limit DSSC development for a variety of reasons, including [19–21]: The first is a poor electron mobility, which leads to a high rate of combination and restricts efficiency increase; the second is an expensive method of producing nanostructures for further dye absorption per unit volume increase, thirdly, a conventional technique for synthesis of anatase TiO_2 normally necessitates high-temperature post-treatments such as annealing, which is commonly employed to remove additives and increase photoanode porosity and/or crystallization of the metal oxide [22,23].

2.1.3 Factors that Govern the Performance of Dye-Sensitized Solar Cells

The much lower efficiency and stability is the big hindrance for the performance of DSSCs to make it comparable to other solar cell types. The performance of DSSCs is influenced by a number of variables. The three most important aspects are listed below [5,6]:

- Poor light absorption;
- Sub-par photovoltage output; and
- Low fill factors.

The dye sensitizers used in DSSCs have a limited spectrum response, which accounts for the inefficient light absorption [6]. Charge recombination is an account for the poor fill factor values, while losses in series resistance are an account for the sub-par photovoltage [5]. Although there are some common dyes such as N719 dye, which have been reported to have substantial efficiency ranging 11-12 percent for titania based DSSCs. But still there are some problems associated with these dyes such as optimization of absorption spectra for high conversion efficiencies. These dyes possesses 15 to 20 mA/cm^2 current densities because of less absorption range which usually cannot be achieved higher than 800nm [6].

To achieve current densities exceeding 25 mA/cm^2 and considerably increase the efficiency and stability of DSSCs, a collaborative effort is required to synthesize new dyes with a broader spectrum response. [22,23]. There has already been some effort

done to synthesize novel dyes with greater molar extinction coefficients and a broader spectrum response, enabling for better light harvesting and stability, such as ruthenium-based K-19. These new dyes are regarded to be extremely promising in the search for DSSC efficiency greater than 12%.[25].

Some researchers have reported that there is some window to increase the efficiency up to 50 % by reducing the recombination rate being happen in the interface of metal oxide and electrolyte. There are few recommended approaches to enhance open circuit voltage which are introduction of barrier layer which can help to interfacial recombination. Another approach is exploration of new electrolytes with Co-adsorbents [24].

High fill factor values indicate good-performing DSSCs. Fill factor limitations are mostly caused by series resistance losses. As a result, it's thought that manipulating the contact between the two electrodes, as well as between wires that connect the electrodes, might affect the amount of series resistance. In addition to these three regulating factors, the semiconductor film morphology and fabrication conditions can have a significant impact on the conversion efficiency of DSSCs. It is critical that the semiconducting nanomaterial's surface area be as large as feasible. The efficiency of DSSCs is also based on particle size, larger the particle size can enhance the red-light absorption in some cases and this red light absorption takes place through light scattering which can further reduce the surface area. The construction of a multilayer TiO_2 morphology for producing a DSSC that balances the conflicting effects of light scattering and surface area was detailed by *Wang et al.* and the cell's effectiveness was improved because to their recommended morphology [26].

The thickness of the film is another component of its shape. DSSCs performance is largely effected by thickness of photoanode thin film. A study was conducted by *Giannouli et al.* with Rose Bengal and Rhodamine B sensitizers. The main purpose of study was to reveal the fact how the efficiency of DSSCs is effected by ZnO film thickness. The results showed that there is an optimum thickness to achieve maximum efficiency. Beyond this optimum thickness either less or more thickness can reduce the conversion efficiency [27].

Finally, the processing parameters of the semiconductor film can affect the DSSC's performance. *Lu et al*. investigated the effect of annealing temperature on the

performance of a DSSC based on ZnO nanoparticles. Temperatures ranging from 300°C to 450°C were tested, and 400°C was shown to be the optimal annealing temperature, with the highest IPCE value and 3.92 percent conversion efficiency. Furthermore, *Lu et al*. concluded that a better charge collecting efficiency could be achieved at an annealing temperature of 400°C since this temperature allowed the impacts of bulk traps to be reduced the most [28].

2.2 Why ZnO Based DSSC

TiO_2 nanoparticles were responsible for the development of dye-sensitized solar cells, as previously stated. However, new metal oxide nanomaterials are being studied in order to replace TiO_2 nanoparticles. The metal oxide's requirements are as follows [29].

- It should have a broad bandgap in order to absorb as many photons as feasible
- To enable proper injection of electrons from excited dye molecules, the conduction band's energy level must be properly lower than the dye's HOMO level.
- For effective charge transport, it should have a high charge carrier mobility; and
- It should have a large enough surface area to efficiently adsorb dye molecules.

In the last decade, there has been a lot of research on DSSCs, with various semiconducting metal oxide materials including ZnO being researched [30,31]. In compared to TiO_2 nanoparticle-based DSSCs, the amount of literature on ZnO-based DSSCs is limited. However, there are some advantages of using ZnO. ZnO has similar electron affinity and comparable band gap i.e,~3.2eV for TiO_2 and ~3.3eV for ZnO [30,31]. Electron diffusivity of ZnO is much higher in comparison to TiO_2 [30] and electron mobility of ZnO is high as well i.e. ~115-155 cm^2V-1s-1 [32]. All these properties are promising for effective transport of electrons [33] and for decreasing recombination rate [34] hence proving ZnO an attractive alternative to TiO_2 based photoanodes for fabrication of DSSCs.

To date, numerous work has been done to improve overall performance of DSSCs; firstly, through improved mesoporous photoanode's light trapping capabilities [18,35], secondly, via surface changes to improve dye adsorption as well as reduce recombination [36,37].A variety of ZnO nanostructures can be grown easily by using

simple and low cost methods (e.g., ZnO nanowires) has been proposed that can be used instead of TiO_2 nanoparticles due to the following reasons [38].

- Electrons can follow in a direct conduction path from the point of injection to the point of collection owing to the nanowire morphology, and
- The surface area of the nanowires is sufficient for dye adsorption.

The rate of injection of electrons in nanowire based photoanode is fast due to the 1-d structure and diffusivity specially for ZnO nanowires. Many researchers reported that nanowires possess 10 to 15 percent more electron transport in comparison to titania nanoparticles. Which can be due to the high crystallinity and electric field present internally that can facilitate the transport of electrons to conducting glass. These attributes can help to separate the electrons of electrolyte oxidized specie. As a result, the charge electron collecting efficiency is improved [39]. Furthermore, ZnO-based nanomaterials can be synthesised at low temperatures, allowing for the use of a variety of substrates, including polymers, and lowering energy costs. The best efficiency achieved by a ZnO-based DSSC as a photoanode to date is 7%, however this was achieved using 1D multilayer ZnO nanowire arrays. Another study found a 4.8 percent efficiency, which was unique in its synthesis, which included a hierarchal structure of ZnO nanosheets and nanowires [40]. DSSCs with only one layer of ZnO nanowire arrays have efficiencies ranging from 0.1-3 percent, according to reports. [31–33].

2.3 Problem Statement

Apart from the stability issue, there are many other factors such as electron conduction and dye adsorption, which effect the overall performance of DSSCs. However, researchers have worked in this direction to address these issues, Chang et al. has achieved 70% of initial efficiency after more than 1 year [44]. Growth of different nanostructures have also addressed these issues up to some extent and further investigation is needed to explore the different synthesis techniques and their resulted products for overall performance of DSSCs. A previously reported synthesis process for ZnO nanoparticles [45] was employed to synthesize different nanostructures by changing the solvent and molar concentration to check the behavior of ZnO grown nanostructures and investigate the overall performance. A previous study proven that amine based alkali and Zinc acetate solution in water gives the product (nanoprisms) and also recommended that amine based alkali can also be replaced with other alkali

solutions and the changes in morphology can be investigated [36,37]. Solvents like water allow a high number of functional atoms along a, b, and c-axis favoring the growth of wurtzite hexagonal crystal structure of ZnO in all possible directions with lower aspect ratio [48]. So, in this project we expected the growth of nanoprism or low aspect ratio nanorods in water and 1D nanostructures like wires or high aspect ratio nanorods in organic solvent (ethanol/methanol) to improve dye loading, reduce recombination as well as will to add benefits towards the stability issue, in a whole an improved overall performance of DSSCs is expected.

Summary

This chapter starts with highlighting the basics of dye sensitized solar cells. And then the focused was shifted from the basics towards more detailed major problem and their solutions being presented in literature. This chapter also include the reasoning for our selection of the material for our project. All the properties and expected improvements with challenges are discussed in detail for dye sensitized solar cells specially for photoanode material.

References

[1] B. O. Regan and M. Gratzelt, “A low-cost, high-efficiency solar cell based on dye-sensitized colloidal $Ti0_2$ films,” vol. 353, pp. 737–740, 1991.

[2] K. Kakiage, Y. Aoyama, T. Yano, K. Oya, J. I. Fujisawa, and M. Hanaya, “Highly-efficient dye-sensitized solar cells with collaborative sensitization by silyl-anchor and carboxy-anchor dyes,, vol. 51, no. 88, pp. 15894–15897, 2015.

[3] B. O’Regan and M. Grätzel, “A low-cost, high-efficiency solar cell based on dye-sensitized colloidal TiO_2 films, vol. 353, no. 6346, pp. 737–740, 1991.

[4] R. Jose, V. Thavasi, and S. Ramakrishna, “Metal oxides for dye-sensitized solar cells., vol. 92, no. 2, pp. 289–301, 2009.

[5] J. Bisquert, D. Cahen, G. Hodes, S. Rühle, and A. Zaban, “Physical chemical principles of photovoltaic conversion with nanoparticulate, mesoporous dye-sensitized solar cells, vol. 108, no. 24, pp. 8106–8118, 2004.

[6] M. Grätzel, “Dye-sensitized solar cells, vol. 4, no. 2, pp. 145–153, 2003.

[7] V. Thavasi, V. Renugopalakrishnan, R. Jose, and S. Ramakrishna, “Controlled electron injection and transport at materials interfaces in dye sensitized solar cells, vol. 63, no. 3. pp. 81–99, 2009.

[8] P. Piotrowiak, Ed. Cambridge: Royal Society of Chemistry, 2013.

[9] G. Boschloo and A. Hagfeldt, “Characteristics of the iodide/triiodide redox mediator in dye-sensitized solar cells, vol. 42, no. 11, pp. 1819–1826, 2000.

[10] M. Wang *et al.*, “An organic redox electrolyte to rival triiodide/iodide in dye-sensitized solar cells, vol. 2, no. 5, pp. 385–389, 2010.

[11] G. Oskam, B. V. Bergeron, G. J. Meyer, and P. C. Searson, “Pseudohalogens for dye-sensitized TiO_2 photoelectrochemical cells, *B*, vol. 105, no. 29, pp. 6867–6873, 2001.

[12] A. Yella *et al.*, “Porphyrin-sensitized solar cells with cobalt (II/III)$^-$based redox electrolyte exceed 12 percent efficiency, vol. 334, no. 6056, pp. 629–634, 2011.

[13] M. Grätzel, “Photoelectrochemical cells, vol. 414, no. 6861, pp. 338–344, 2001.

[14] J. B. Baxter and E. S. Aydil, “Dye-sensitized solar cells based on semiconductor

morphologies with ZnO nanowires," vol. 90, no. 5, pp. 607–622, 2006.

[15] N. Papageorgiou, "Counter-electrode function in nanocrystalline photoelectrochemical cell configurations, vol. 248, no. 13–14. pp. 1421–1446, 2004.

[16] S. Yun, A. Hagfeldt, and T. Ma, "Pt-free counter electrode for dye-sensitized solar cells with high efficiency, vol. 26, no. 36, pp. 6210–6237, 2014.

[17] P. R. F. Barnes *et al.*, "Interpretation of optoelectronic transient and charge extraction measurements in dye-sensitized solar cells, vol. 25, no. 13. John Wiley & Sons, Ltd, pp. 1881–1922, 2013.

[18] F. Huang, D. Chen, X. L. Zhang, R. A. Caruso, and Y. B. Cheng, "Dual-function scattering layer of submicrometer-sized mesoporous TiO_2 beads for high-efficiency dyesensitized solar cells, vol. 20, no. 8, pp. 1301–1305, 2010.

[19] M. K. Nazeeruddin *et al.*, "Conversion of Light to Electricity by cis-X2Bis (2,2′-bipyridyl-4,4′-dicarboxylate) ruthenium (II) Charge-Transfer Sensitizers (X = Cl−, Br−, I−, CN−, and SCN−) on Nanocrystalline TiO_2 Electrodes," vol. 115, no. 14, pp. 6382–6390, 1993.

[20] P. M. Sommeling *et al.*, "Influence of a $TiCl_4$ post-treatment on nanocrystalline TiO 2 films in dye-sensitized solar cells , vol. 110, no. 39, pp. 19191–19197, 2006.

[21] S. Ito *et al.*, "Control of dark current in photoelectrochemical (TiO_2/I^--I^{3-}) and dye-sensitized solar cells, no. 34, pp. 4351–4353, 2005.

[22] Q. Zhang and C. Li, "High temperature stable anatase phase titanium dioxide films synthesized by mist chemical vapor deposition, vol. 10, no. 5, 2020.

[23] P. Periyat, B. Naufal, and S. G. Ullattil, "A review on high temperature stable anatase TiO_2 photocatalysts, vol. 855, pp. 78–93, 2016.

[24] P. Wang, C. Klein, R. Humphry-Baker, S. M. Zakeeruddin, and M. Grätzel, "A high molar extinction coefficient sensitizer for stable dye-sensitized solar cells," vol. 127, no. 3, pp. 808–809, 2005.

[25] M. K. Nazeeruddin, C. Klein, P. Liska, and M. Grätzel, "Synthesis of novel ruthenium sensitizers and their application in dye-sensitized solar cells, vol.

249, no. 13–14, pp. 1460–1467, 2005.

[26] Z. S. Wang, H. Kawauchi, T. Kashima, and H. Arakawa, "Significant influence of TiO_2 photoelectrode morphology on the energy conversion efficiency of N719 dye-sensitized solar cell, vol. 248, no. 13–14. pp. 1381–1389, 2004.

[27] M. Giannouli and F. Spiliopoulou, "Effects of the morphology of nanostructured ZnO films on the efficiency of dye-sensitized solar cells, vol. 41, pp. 115–122, 2012.

[28] D. Zhao, T. Peng, L. Lu, P. Cai, P. Jiang, and Z. Bian, "Effect of annealing temperature on the photoelectrochemical properties of dye-sensitized solar cells made with mesoporous TiO_2 nanoparticles, vol. 112, no. 22, pp. 8486–8494, 2008.

[29] H. J. Snaith and L. Schmidt-Mende, "Advances in liquid-electrolyte and solid-state dye-sensitized solar cells, vol. 19, no. 20, pp. 3187–3200, 2007.

[30] R. Vittal and K. C. Ho, "Zinc oxide based dye-sensitized solar cells: A review," vol. 70, pp. 920–935, 2017.

[31] P. S. Archana, R. Jose, C. Vijila, and S. Ramakrishna, "Improved electron diffusion coefficient in electrospun TiO_2 nanowires, vol. 113, no. 52, pp. 21538–21542, 2009.

[32] E. M. Kaidashev *et al.*, "High electron mobility of epitaxial ZnO thin films on c-plane sapphire grown by multistep pulsed-laser deposition, vol. 82, no. 22, pp. 3901–3903, 2003.

[33] N. A. Karim, U. Mehmood, H. F. Zahid, and T. Asif, "Nanostructured photoanode and counter electrode materials for efficient Dye-Sensitized Solar Cells (DSSCs), vol. 185, pp. 165–188, 2019.

[34] R. Ansir, N. Ullah, B. Ünlü, S. Mujtaba Shah, and M. Özacar, "Effect of annealing temperatures on performance of DSSCs fabricated using Ag or Pd@C@ZnO composites as photoanode materials, vol. 224, pp. 617–628, 2021.

[35] T. T. T. Pham, N. Mathews, Y. M. Lam, and S. Mhaisalkar, "Enhanced Efficiency of Dye-Sensitized Solar Cells with Mesoporous–Macroporous TiO_2 Photoanode Obtained Using ZnO Template, vol. 46, no. 6, pp. 3801–3807,

2017.

[36] A. Wibowo *et al.*, "ZnO nanostructured materials for emerging solar cell applications, vol. 10, no. 70, pp. 42838–42859, 2020.

[37] P. M. Sommeling *et al.*, "Influence of a $TiCl_4$ post-treatment on nanocrystalline TiO_2 films in dye-sensitized solar cells, vol. 110, no. 39, pp. 19191–19197, 2006.

[38] J. B. Baxter and E. S. Aydil, "Nanowire-based dye-sensitized solar cells., vol. 86, no. 5, pp. 1–3, 2005.

[39] M. Law, L. E. Greene, J. C. Johnson, R. Saykally, and P. Yang, "Nanowire dye-sensitized solar cells, vol. 4, no. 6, pp. 455–459, 2005.

[40] F. Xu, M. Dai, Y. Lu, and L. Sun, "Hierarchical ZnO nanowire-nanosheet architectures for high power conversion efficiency in dye-sensitized solar cells, vol. 114, no. 6, pp. 2776–2782, 2010.

[41] C. Xu, P. Shin, L. Cao, and D. Gao, "Preferential growth of long ZnO nanowire array and its application in dye-sensitized solar cells, vol. 114, no. 1, pp. 125–129, Jan. 2010.

[42] J. B. Baxter, A. M. Walker, K. Van Ommering, and E. S. Aydil, "Synthesis and characterization of ZnO nanowires and their integration into dye-sensitized solar cells, vol. 17, no. 11, 2006.

[43] J. B. Baxter and E. S. Aydil, "Dye-sensitized solar cells based on semiconductor morphologies with ZnO nanowires, vol. 90, no. 5, pp. 607–622, 2006.

[44] W. C. Chang, C. H. Lee, W. C. Yu, and C. M. Lin, "Optimization of dye adsorption time and film thickness for efficient ZnO dye-sensitized solar cells with high at-rest stability, vol. 7, no. 1, pp. 1–10, 2012.

[45] P. M. Aneesh, K. A. Vanaja, and M. K. Jayaraj, "Synthesis of ZnO nanoparticles by hydrothermal method, vol. 6639, p. 66390J, 2007.

[46] J. M. Hancock, W. M. Rankin, B. Woolsey, R. S. Turley, and R. G. Harrison, "Controlled formation of ZnO hexagonal prisms using ethanolamines and water, vol. 84, no. 1, pp. 214–221, 2017.

[47] Y. Liu, H. Liu, Q. Zhang, and T. Li, "Adjusting the proportions of {0001} facets

and high-index facets of ZnO hexagonal prisms and their photocatalytic activity, vol. 7, no. 6, pp. 3515–3520, 2017.

[48] A. Ejaz, J. H. Han, and R. Dahiya, “Influence of solvent molecular geometry on the growth of nanostructures, vol. 570, pp. 322–331, 2020.

Chapter 3

Material Processing and Characterization Techniques

3.1 Material Preparation

To synthesize ZnO nanostructured materials, a wide range of synthesis techniques have been documented. The preparation conditions have a big impact on the ZnO characteristics. Synthesis processes are divided into two categories; High temperature (Chemical and Physical Vapor deposition) and low temperature (Hydrothermal or electrochemical deposition).

3.1.1 Vapor Phase methods

For the synthesis of ZnO nanostructures, vapor phase approaches have been widely used. Thermal evaporation is usually carried out in a tubular furnace at a high temperature (about 1000°C) and in most cases under vacuum conditions. The produced ZnO nanostructures' form and phase structure are influenced by the source materials and reaction conditions.

Temperature, pressure, carrier gas, substrate, and evaporation time period are all factors to consider. The vapour phase process begins with the evaporation of material by heating it above its eutectic temperature and transporting it with a carrier gas to a lower-temperature chamber of the furnace where a substrate is placed [1].

The vapors are then condensed into solid material on top of the substrate of choice. There are numerous distinct types of vapor phase deposition processes, which can be classified into two categories: chemical vapor deposition (CVD) (Fig. 3.1) and physical vapor deposition (PVD) (Fig. 3.2).

In CVD, the starting material reacts on the substrate's surface to produce the desired solid material, whereas in PVD, the target material is simply evaporated and re-condensed to a solid state [1].

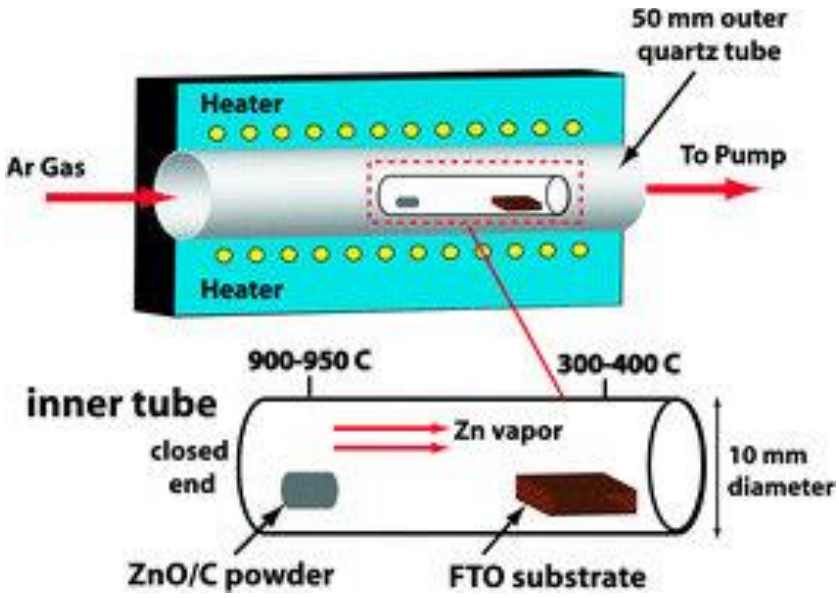

Fig. 3.1: Schematic representation of CVD system with double-tube configuration [1]

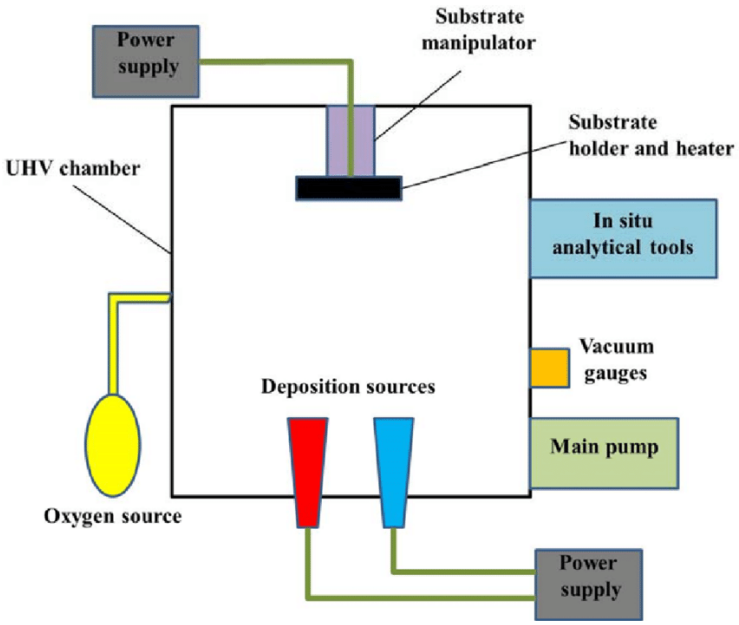

Fig. 3.2: Schematic representation of PVD system [2]

3.1.2 Electrochemical deposition synthesis (ED)

In an aqueous growth solution, electrochemical deposition (ED) is a low-temperature method. A three-electrode arrangement is used in the classic ED reaction, with an Ag/AgCl reference electrode and a Pt counter-electrode [3]. The substrate is used as a working electrode where deposition of ZnO occurs. A constant voltage source or a constant current source controls the reaction system to maintain a constant driving force or reaction rate. A dissolved Zn^{2+} salt as well as an oxygen source (O_2 or NO_3) are required in the aqueous solution. The rate of ZnO synthesis is determined by the

precursor concentrations as well as the voltage or current used in the process. Templated growth is a synthetic process that combines ED with templates such as anodic aluminum oxide (AAO). This allows for precise control of the dimensions of the synthesized ZnO nanostructures [4].

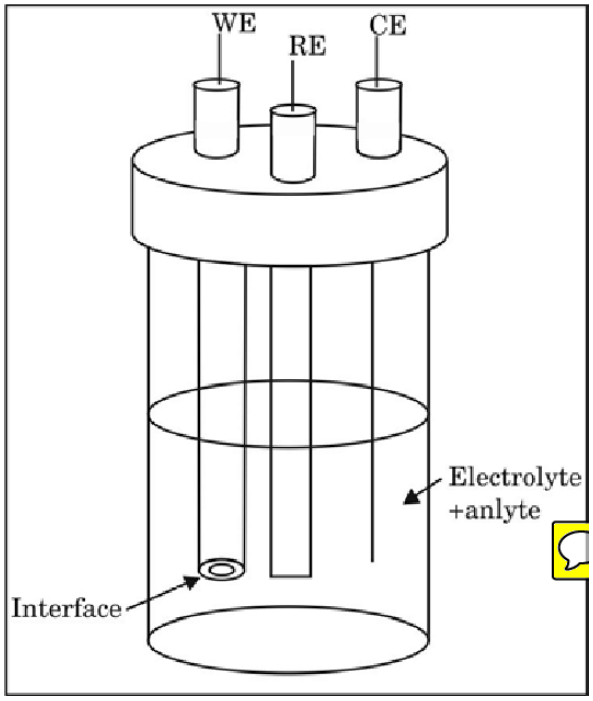

Fig. 3.3: Illustration for the three-electrode setup used in the electrochemical techniques. WE = Working electrode; RE= Reference electrode; CE= Counter electrode [5]

3.1.3 Hydrothermal and chemical bath deposition

Hydrothermal processing one of inorganic synthesis technique in advanced materials in which nanoparticles prepared under low temperature and pressure usually, this technique is involving in preparation of catalysts via using an oven and autoclave. Hydrothermal is also known as chemical bath deposition technique. The hydrothermal process involves forming ZnO by hydrolyzing Zn^{+2} salts in a basic aqueous solution. Strong or weak alkali can also be used to create ZnO nanostructures.

Hexamethylenetetramine (HMTA) is the most commonly utilized base, which acts as a pH buffer and maintains a pH of 6-7 to gently deliver anion. NaOH, KOH, and NH_4 are some of the other bases employed in hydrothermal synthesis. When solution is heated, the precipitation of ZnO begins when the concentration of both Zn^{+2} and OH^{-1} surpass a critical amount. The final ZnO nanostructure, size, and quality are determined

by hydrothermal synthesis parameters such as zinc concentration in solution, growth time, and growth temperature. [6].

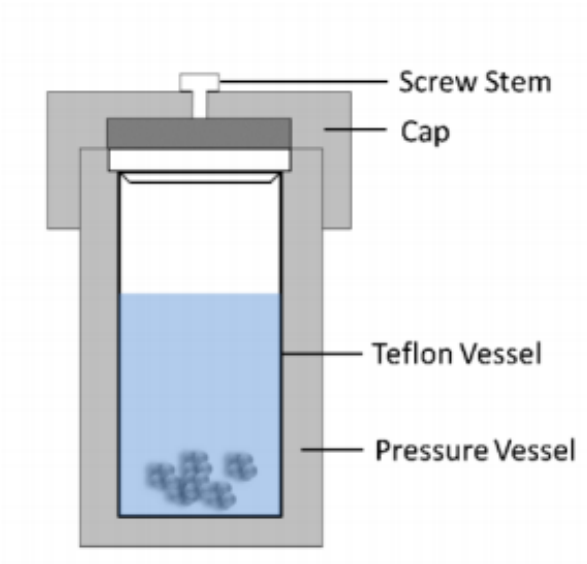

Fig. 3.4: Teflon lined autoclave for hydrothermal [6]

3.2 Nanostructures Characterization

The results attained by using various characterization techniques;

- X-rays diffraction
- Scanning electron microscopy
- Ultraviolet-Visible spectroscopy

3.2.1 X-Ray powder diffraction

X-Ray Diffraction analysis instrument has very significant and valuable apparatus which characterized the various specimens, to observed lattice parameter as well as for analysis of crystalline phase, and their alignment. Catalysts are extensively studied and characterized. X-ray diffractometry (XRD) of powder was performed on XRD apparatus (Bruker, D8 advanced) employing a Cu Kα radiation (λ = 1.5418 Å) source and fitted with a 25-kV power. The data was collected in the range of 20 - 70° of 2θ with the step-scan of 0.02°. X-ray diffraction (XRD) is the most nondestructive technique to explore structural characteristics of a material. XRD is examined internal structure properties of a material by employing X-rays on material. X-ray diffraction (XRD) technique is used to determine different morphological and structural information of synthesized nanomaterials.

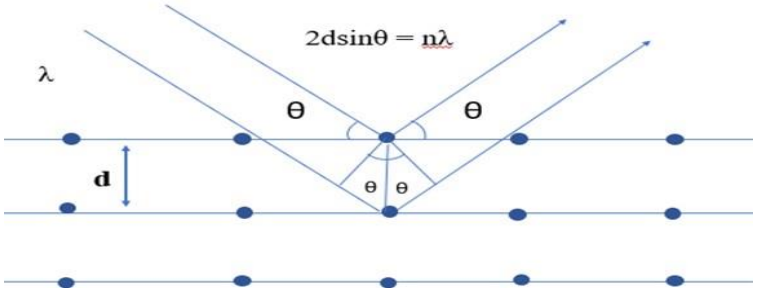

Fig. 3.5: X-ray diffraction of crystal lattice planes having layers of material adopted from reference [7].

This technique is well known for determination of phase purity and dimensions of crystalline materials in field of material science. This technique is provided information about atoms positions and symmetry shape, size and atomic spacing of atoms in unit cell of solid materials. Crystalline material and the interference x-rays are the result of specimens given by this technique [7]. In x-ray diffraction technique, through cathode ray tube generation of x-rays occurs and after the process of filtration, monochromatic light is emitted. This monochromatic light is concentrating to sample material. When incident rays interact to sample it makes constructive interference and following Bragg's law [8]:

$$2d\sin\theta = n\lambda \qquad (3.1)$$

Integer is identified by alphabet n, while λ represent X-ray wavelength, the interplanar spacing of catalyst that results in diffraction is d and u is actually the angle of diffraction. Bragg' law helps to recount the electromagnetic radiation wavelength according to diffraction angle and spacing lattice crystalline sample. During X-ray powder diffraction, the scanning made incident angle that varied from 10° to 80° at scanning rate of 10° per min using Cu Kα radiations λ =1.5405 Å. After diffraction x-rays are then easily identified and calculated.

A filament is heated by the applying voltage to the cathode ray tube that emits x-rays to generate electrons. These accelerated electrons are bombarded on the surface of a sample. When these accelerated electrons have gained adequate energy to remove the inner shell electrons to move them a higher energy level after that these electrons lose their energy, move to low energy level by emitting a photon. The emitted photons with a specific wavelength show the characteristic of sample material. Through analysis of x- ray emission spectrum which give qualitative results about the structure of sample

material. These spectra contain on different components, the most common being K_α and K_β [8].

3.2.2 Scanning electron microscopy (SEM)

SEM is an electron microscope type which capable of developing high resolution images of sample. In its image have three-dimensional appearance and useful for surface structure observation sample. The different morphologies of Zinc oxide Nanostructure were observed by using SEM. The schematic of its working is shown below.

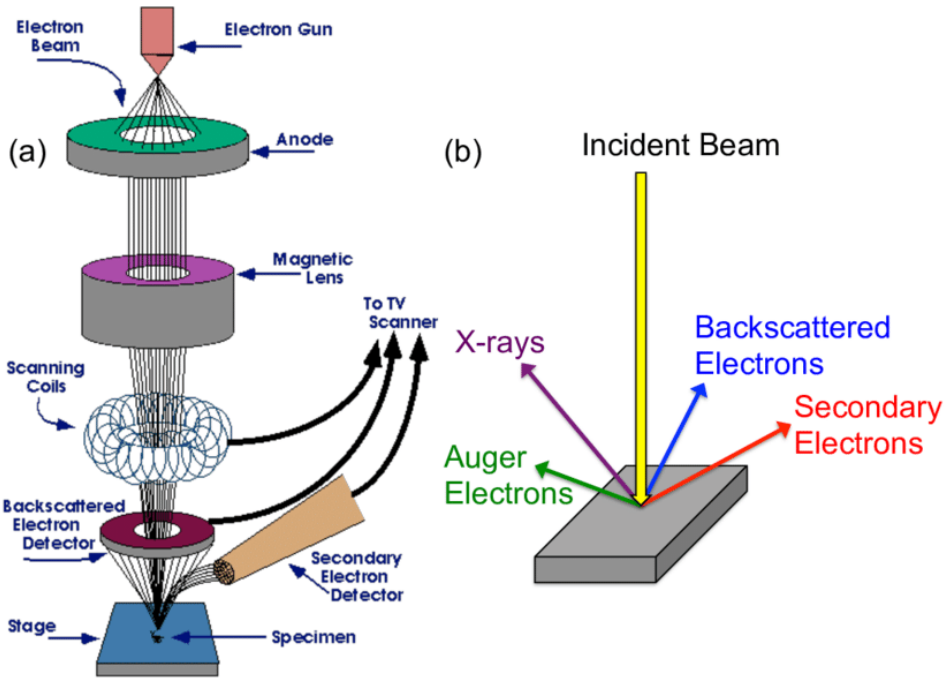

Fig. 3.6: Schematic drawing of Scanning Electron Microscope (SEM) [9]

The electrons produced by the hot filament acquired by electric and magnetic fields. These excited electrons by interact with sample material to initiate the signals and these signals are containing the information of surface morphologies of materials. The scanning electron microscopy is an analytical technique which is used to examine the external morphologies, shapes, chemical composition, size and arrangements of atoms that making up the samples. In this technique, when sample hit with a beam of high energy electrons, which is known as incident beam that strike the surface of solid sample to generate secondary electrons (signals). These secondary electrons are counted by positive charged electron detector which reveal two or three-dimension image of sample including information regarding variety of shapes, size, composition

and topography of the sample [9]. The size and the shape of nanostructures was studied by using scanning electron microscopy (TESCAN-VEGA-3). SEM images were examined with a magnification of 5µm-500nm with an accelerating voltage of 15.0-10.0kV.

Energy dispersive X-ray spectroscopy (EDS) allows the target surface analysis and widely used for material surface analysis. This provides the elemental identification and quantitative compositional information. EDS analysis are performed on the same apparatus as for SEM (TESCAN-VEGA-3) by adjusting voltage at 20kV and width 15mm. IR camera view was turned off to acquire the spectrum for site of interest.

3.2.3 UV-Vis spectroscopy

The optical measurements of structures like absorbance were found by using the measured diffuse reflectance of nanostructures deposited over glass substrate by using ultraviolet-visible (UV-Vis) spectrophotometer (PerkinElmer, Lambda 950). UV-visible spectroscopy also known as "electronic spectroscopy" is a technique used to determine the bandgap energy of the semiconductor employed for the photo-activity. The absorption of UV-visible irradiation from a specimen can be determine by ultra violet-visible spectroscopy with a single wave lengths or scans over a range within a spectrum. The UV light wavelength lengthen from 200-400 nm while the wavelength of visible spectrum ranges from 400-800 nm. The concentration of an electromagnetic energies from UV-visible spectrum stimulates an electron fervor from conduction to valance energy states. The light absorbance of any absorbing substance is basically directed through Lambert-Beer law which defines as while keeping the specimen thickness constant, when a radiation of particular wavelength passes through the compartment of sample, it causes in the absorbance of light that gives the results.

The Lambert-Beer Law, mathematically can be formulated as follows [10];

$$\mathbf{A = \text{Ɛ}lc} \qquad \mathbf{(3.\ 2)}$$

Where, A is absorbance or optical density,

Ɛ is epsilon (molar absorption coefficient of the analyte having certain wavelength),

l is path length of the specimen,

c is the concentration of analyte.

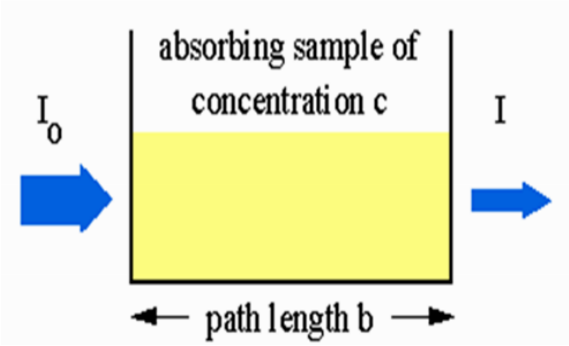

Fig. 3.7: Basic Principle of Lambert-Beer Law [11]

I_0 is the concentration of incident light and I is the concentration of light after passing through the sample.

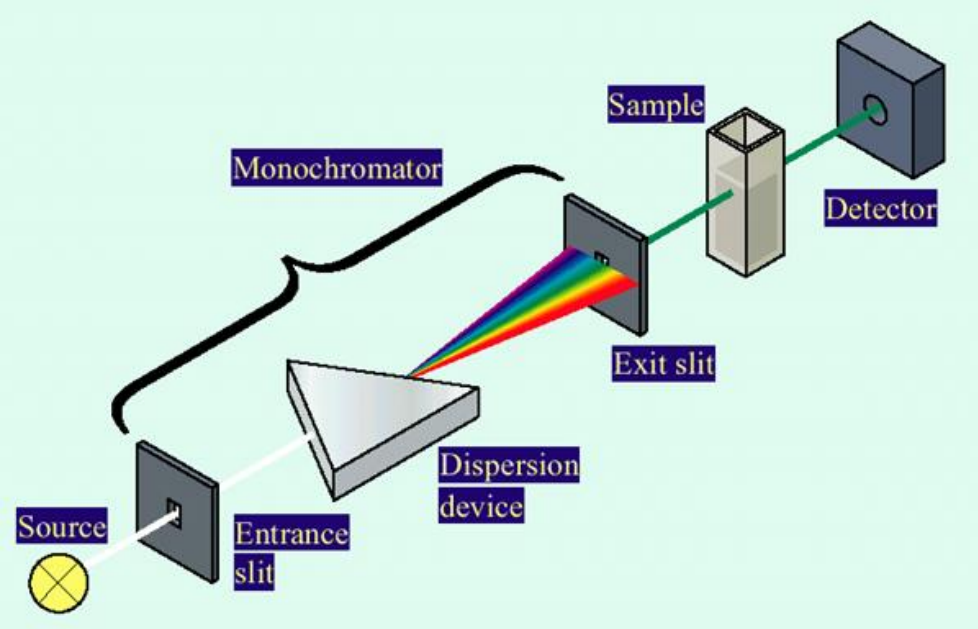

Fig. 3.8: Fundamental Principle of UV-Vis Spectroscopy [10]

Band gap analysis

The spectrum of UV-Vis used to calculate the energy band gap of gap, through this is determines the relationship between absorption coefficient by the absorption edge and the optical band gap. Diffuse reflectance spectra is the simple way to measure the band gap this study, Kubelka-Munk model is the foremost way for band gap analysis [12]. Following equation being followed;

$$(\alpha h\nu)2 = (h\nu - Eg) \qquad (3.3)$$

α = Absorption constant, based on the effective masses related with the VB and CB

hv = Photon Energy

3.2.4 Brunauer-Emmett-Teller (BET) surface area analysis

Porosity and adsorption study of grown structures was conducting with the help of Brunner-Emmett-Teller (BET) surface area analyzer (NOVA, Quantachrome). The Brunauer–Emmett–Teller (BET) theory is a critical analytic technique to measuring material specific surface area that aims to explain the physical adsorption of gas molecules on a solid surface. Physical adsorption, or physisorption, is the term for this phenomenon. The BET theory is used to determine specific surface area in multilayer adsorption systems, and it typically uses probing gases (named adsorbents) that do not chemically react with material surfaces like adsorbates (the material onto which the gas adheres and the gas phase is termed the adsorptive). The most often utilized gaseous adsorbate for surface probing is nitrogen [13].

3.3 DSSCs Fabrication Techniques

Two DSSCs fabrication techniques are commonly used

- Sealed
- Microfluidic Structure

3.3.1 Sealed

In this technique, a sandwich like cell is prepared by using metal oxide working electrode and a hole drilled counter electrode in a way both remained in face-to-face position. A 30 μm thick surlyn thermoplastic is used as a sealant and adjusted in a way that inner dimensions should match with the active area of cell of working electrode. Final sealed DSSC is fabricated by employing heat with holes in counter electrode for the introduction of electrolyte [14].

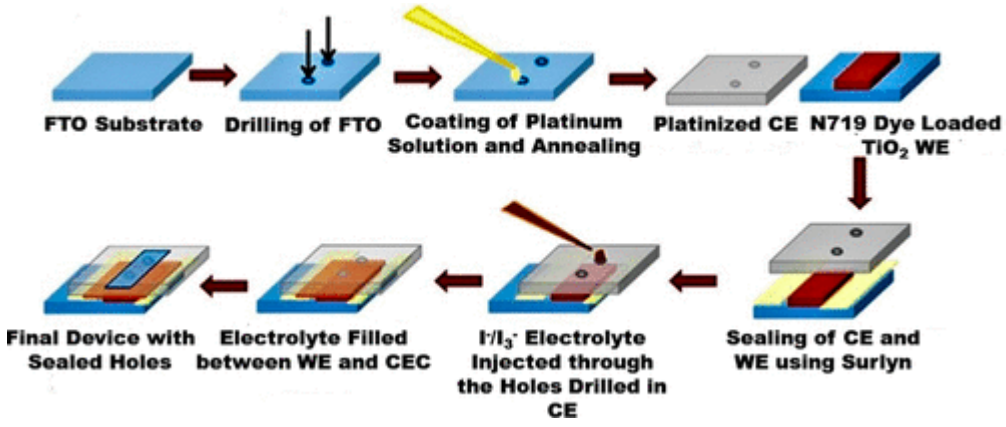

Fig. 3.9: Schematic illustration of the stepwise procedure of DSSC fabrication [14]

3.3.2 Microfluidic

Microfluidic structure is reusable clamping system used for DSSCs fabrication guaranteed the sealing to avoid leakage of electrolyte. In this fabrication technique two polymethylmethacrylate (PMMA) external clamping structures used with holes for screw tightening to hold all the components in place. PDMS pre-polymer and curing agent is used a membrane sandwiched between photoanode and counter electrode. Photoanode and counter electrodes are placed on PMMA structures in a way allowing electrolyte to be flow in between the electrodes through housing ports. Copper foils are used to make connections for both photoanode and counter electrode [15].

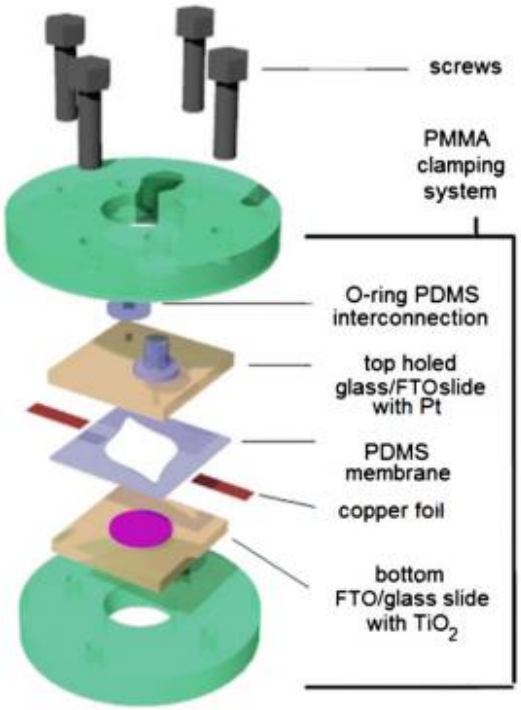

Fig. 3.10: Scheme of the microfluidic dye-sensitized solar cell [15]

3.4 DSSC Characterization

3.4.1 Photovoltaic Characterization

Newport Oriel IV station with Kiethley PVIV 2400 source meter and solar simulator under power intensity of 750 W/m2 were used for IV measurements. External quantum efficiency (EQE) for each cell was measured by using quantum efficiency measurement system (Enlitech, QE-R). While the cell was covered with a black mask having an active area of 0.22 cm^2 to limit extra light [16]. The simulator's output light intensity was calibrated (1000 Wm^{-2}) using a reference Si photodiode that Newport

had calibrated at (1000 W m^{-2}). Important characteristics such as open circuit voltage (Voc), short circuit current density (Jsc), fill factor (FF), and photo conversion efficiency can be calculated using the J-V data measured for samples.

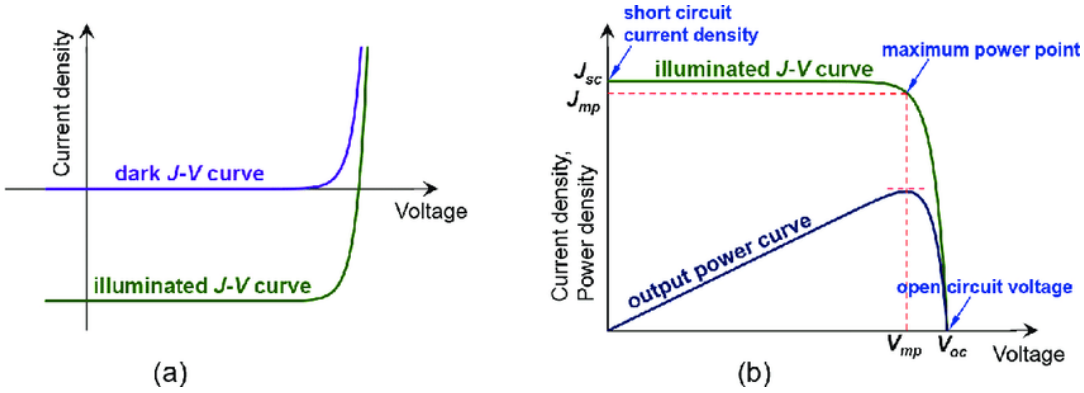

Fig. 3.11: Typical J-V curves under light and dark conditions [17]

Summary

In this chapter, brief description about material preparation technique used and theoretical background of experimental techniques are given. The detailed description is written about instrumental setup and basic principle used for the analyzing of morphology, chemical composition, optical properties and IV characteristics of Zinc oxide nanostructures based DSSCs.

References

[1] D. Yu, T. Trad, J. T. McLeskey, V. Craciun, and C. R. Taylor, "ZnO nanowires synthesized by vapor phase transport deposition on transparent oxide substrates, vol. 5, no. 8, pp. 1333–1339, 2010.

[2] Y. Wang, W. Chen, B. Wang, and Y. Zheng, "Ultrathin ferroelectric films: Growth, characterization, physics and applications, vol. 6, no. 9. pp. 6377–6485, 2014.

[3] T. Yoshida *et al.*, "Electrodeposition of Inorganic/Organic Hybrid Thin Films, vol. 19, no. 1, pp. 17–43, 2009.

[4] S. Xu and Z. L. Wang, "One-dimensional ZnO nanostructures: Solution growth and functional properties, vol. 4, no. 11, pp. 1013–1098, 2011.

[5] M. Grätzel, "Photoelectrochemical cells, vol. 414, no. 6861. Nature Publishing Group, pp. 338–344, 2001.

[6] G. Yang and S. J. Park, "Conventional and microwave hydrothermal synthesis and application of functional materials: A review, vol. 12, no. 7, 2019.

[7] X. Zhou *et al.*, "XRD-based quantitative analysis of clay minerals using reference intensity ratios, mineral intensity factors, Rietveld, and full pattern summation methods: A critical review, vol. 3, no. 1, pp. 16–29, 2018.

[8] A. A. Bunaciu, E. gabriela Udriştioiu, and H. Y. Aboul-Enein, "X-Ray Diffraction: Instrumentation and Applications, vol. 45, no. 4, pp. 289–299, 2015.

[9] L. A. Bulla, G. Julian, C. W. Hesseltine, and F. L. Baker, "Scanning Electron Microscopy, vol. 8, no. C, pp. 1–33, 1973.

[10] I. S. Lyal'ko *et al.*, "Em-125 Transmission Electron Microscope., vol. 47, no. 6, pp. 13–15, 1981.

[11] "Beer-Lambert Law." http://life.nthu.edu.tw/~labcjw/BioPhyChem/Spectroscopy/beerslaw, 2021.

[12] P. Makuła, M. Pacia, and W. Macyk, "How To Correctly Determine the Band Gap Energy of Modified Semiconductor Photocatalysts Based on UV-Vis Spectra, vol. 9, no. 23, pp. 6814–6817, 2018.

[13] G. Fagerlund, “Determination of specific surface by the BET method, vol. 6, no. 3, pp. 239–245, 1973.

[14] A. Roy, A. Ghosh, S. Bhandari, P. Selvaraj, S. Sundaram, and T. K. Mallick, “Color Comfort Evaluation of Dye-Sensitized Solar Cell (DSSC) Based Building-Integrated Photovoltaic (BIPV) Glazing after 2 Years of Ambient Exposure, vol. 123, no. 39, pp. 23834–23837, 2019.

[15] A. Sacco *et al.*, “Microfluidic housing system: A useful tool for the analysis of dye-sensitized solar cell components, vol. 109, no. 2, pp. 377–383, 2012.

[16] C. Zhao *et al.*, “Low temperature growth of hybrid ZnO/TiO_2 nano-sculptured foxtail-structures for dye-sensitized solar cells, vol. 4, no. 105, pp. 61153–61159, 2014.

[17] Y. Tao, “Screen-Printed Front Junction n-Type Silicon Solar Cells, 2016.

Chapter 4
Experimental

4.1 Material and reagents

The ZnO nanomaterials are synthesized through hydrothermal method. The chemical reagents that were used for synthesis of ZnO catalysts nanomaterials, were purchased from Sigma-Aldrich and of laboratory grade with high purification and not required further purification. Zinc acetate di hydrate was used as a precursor for ZnO nanostructure synthesizing. As an alkali base NaOH was used. Deionized (DI) water and alcohol were utilized for synthesis of catalysts as a solvent and for cleaning purposes.

4.2 Glassware and instrumentation

Glassware used for nanoparticles fabrication were beakers, disposable pippets, spatula, magnetic stirrer, glass samples bottles, Eppendorf tubes, centrifuge tubes, nitrile gloves, mask, and goggles. pH meter was used for identification of pH. Hot plate, oven and autoclave were used for preparation of white precipitation of ZnO catalyst. BSA224S Sartorius microbalance was utilized for weighing chemicals. The centrifuge was used for centrifuging the different morphology of ZnO nanostructure.

4.3 Material Synthesis

Fig. 4.1: Schematic diagram of synthesis process

The whole synthesis process is presented schematically in Fig. 4.1 for better understanding. And employed technique for synthesizing nanostructures is briefly discussed in 4.3.1.

The whole synthesis process is summarized in table 4.1.

Table 4.1: Nanostructure's synthesis summary

Sample ID	Solvent for Zinc Acetate	Solvent for NaOH	Drying	Product
Sample 1	Water	Water	At 80 °C for 24 hrs	Nanoprism
Sample 2	Water	Methanol	At 80 °C for 24 hrs	Hollow nanoprism
Sample 3	Methanol	Methanol	At 80 °C for 24 hrs	Nanorice

4.3.1 Hydrothermal Synthesis

Nanostructures were synthesized by using hydrothermal process [1], 1 molar solution of zinc acetate prepared in solvent as shown in table 4.1 and keep on stirring for 20 minutes. 3-5 molar solution of NaOH was also prepared in solvents mentioned in table 4.1 in a separate beaker. A summarized illustration of synthesis process is shown fig. 4.2.

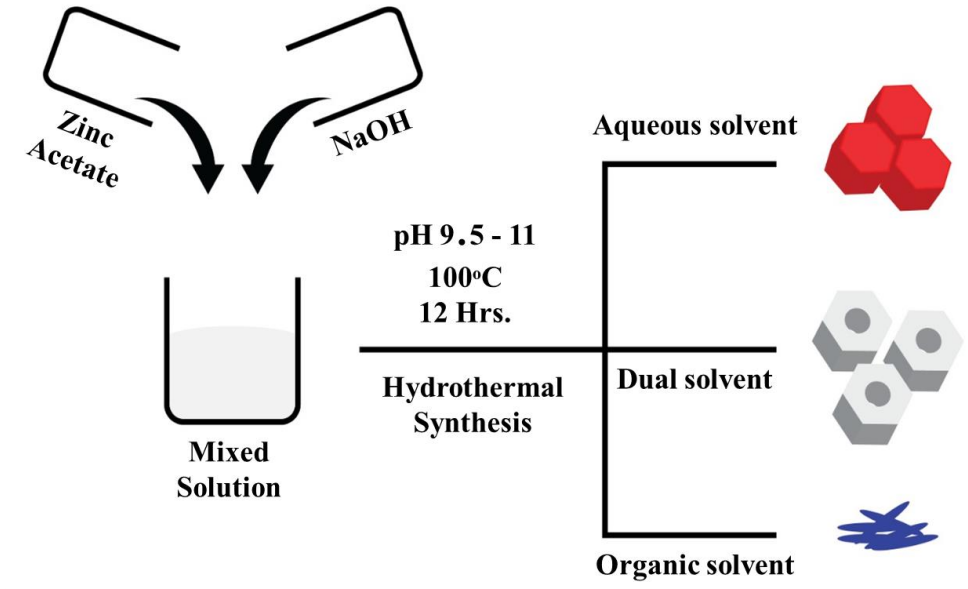

Fig. 4.2: Graphical representation of synthesis process

The alkali solution added dropwise Zinc Acetate solution under continuous stirring. pH of solution kept in range of 9-11, solution transferred into autoclave and kept at 100^{o}C in oven for 24hrs. After 24 hrs, autoclave was allowed to cool down at room temperature. Centrifuge the solution to collect white principates of ZnO. Several times washed precipitates with distilled water and kept on drying for 24 hrs. at 80^{o}C

4.4 Dye sensitized solar cell fabrication

4.4.1 Photoelectrode Preparation

Working electrode was prepared using Fluoride doped tin oxide (FTO) conducting glass as a substrate, which was cleaned in water, isopropanol, acetone and ethanol under sonication for 15 minutes respectively. The cleaned glass was then kept in isopropanol for 24 hours prior to use for film deposition. ZnO paste was prepared using 25mg of photocatalyst mixed with 0.5ml of dimethyl formamide (DMF) [2] containing 25 µL of 5 wt% Nafion to help in adhesion [3] under sonication to make a slurry. The slurry was then dip-coated onto FTO glass substrate and tape casting technique employed to ensure the same thickness. After air drying, the electrode was annealed at 350°C for 30 minutes [4].

Fig. 4.3: Photoanodes

4.4.2 Sensitizing Photoanodes

Photoelectrodes were kept on hot plate at 100^{o}C for 30 minutes and were allowed to cool down for few moments before immersion in dye solution. These samples were soaked into 0.1mM N719 dye solution in an absolute ethanol for 3 hrs at room

temperature. Samples then were rinsed with absolute ethanol to wash out un-adsorbed dye [5].

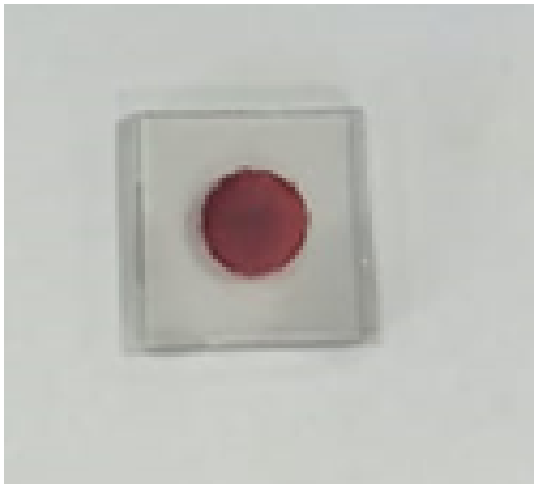

Fig. 4.4: Sensitized photoanodes

4.4.3 Preparation of Pt counter electrodes

Counter electrode was prepared on FTO with hole punched for introduction of electrolyte using Platisol D/SP(Solaronix) solution by doctor blade technique [6]. The holes were drilled through with the help of diamond drilling bit.

4.4.4 Assembling DSSCs

DSSCs were assembled using microfluidic structure [7] with I^-/I^{3-} redox couple electrolyte.

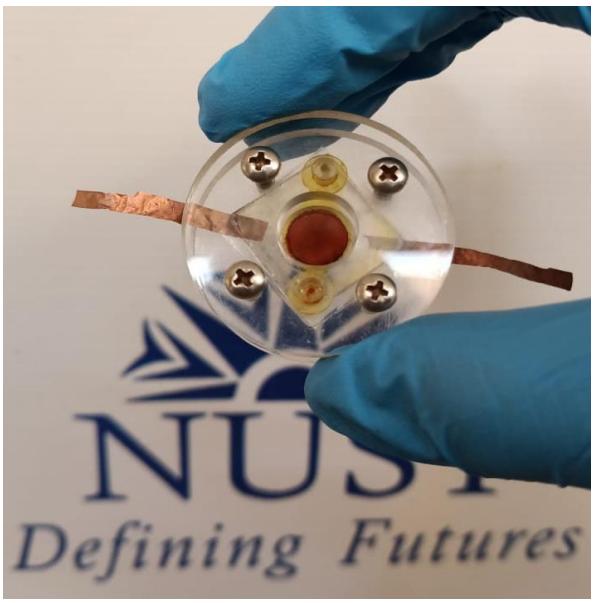

Fig. 4.5: Assembled DSSC

Sensitized photoanode was placed on PMMA clamping system, PDMS was introduced to hold microfluid electrolyte in place for photoanode. A counter electrode was placed in a way allowing electrolyte through the punched holes to flow in between both photoanode and counter electrode within the PDMS. Copper strips were used to make connections for both photoanode and counter electrode. Other side of PMMA clamping system was applied and screws were tightened to hold all the components in place. Electrolyte was introduced with the help of syringe pump through the housing ports[4 – 6]. All the assembled DSSCs having an active area of 0.78cm^2 and electrical measurements were performed by applying a black mask with an active area 0.22cm^2.

Summary

This chapter contains the details of the chemicals, experiment performed in this study, methodology followed for the synthesis of catalysts. It also discusses the synthesis schemes, working conditions, and chemicals stoichiometries for preparation of nanostructures ZnO catalyst in a hydrothermal method. Further, methods employed for the DSSCs fabrication is also listed.

References

[1] B. Liu and H. C. Zeng, “Hydrothermal synthesis of ZnO nanorods in the diameter regime of 50 nm, vol. 125, no. 15, pp. 4430–4431, 2003.

[2] K. Davis, R. Yarbrough, M. Froeschle, J. White, and H. Rathnayake, “Band gap engineered zinc oxide nanostructures: Via a sol-gel synthesis of solvent driven shape-controlled crystal growth, vol. 9, no. 26, pp. 14638–14648, 2019.

[3] F. Lufrano, P. Staiti, and M. Minutoli, “Influence of Nafion Content in Electrodes on Performance of Carbon Supercapacitors, vol. 151, no. 1, p. A64, 2004.

[4] P. Pratim, S. Mukhopadhyay, S. A. Agarkar, A. Jana, and P. S. Devi, “Photochemical performance of ZnO nanostructures in dye sensitized solar cells, vol. 48, pp. 237–243, 2015.

[5] J. Fang, H. Fan, H. Tian, and G. Dong, “Materials Characterization Morphology control of ZnO nanostructures for high efficient dye-sensitized solar cells, vol. 108, pp. 51–57, 2015.

[6] S. Sa, “Platisol T / SP Platisol T / SP,” no. 1, pp. 2–7, 2011.

[7] N. Shahzad *et al.*, “Monitoring the dye impregnation time of nanostructured photoanodes for dye sensitized solar cells, vol. 439, no. 1, 2013.

[8] N. Shahzad *et al.*, “Comparison of hemi-squaraine sensitized TiO_2 and ZnO photoanodes for DSSC applications, vol. 117, no. 44, pp. 22778–22783, 2013.

[9] A. Sacco *et al.*, “Microfluidic housing system: A useful tool for the analysis of dye-sensitized solar cell components, vol. 109, no. 2, pp. 377–383, 2012.

Chapter 5
Results and Discussion

Three samples were prepared to check the influence of solvent on the growth of nanostructures, their behavior and how they affect the performance as photoanode material for dye sensitized solar cells. ZnO nanostructures were synthesized by changing the solvating conditions in a hydrothermal process as illustrated in scheme 1. The change in solvent polarity controls the morphology of the resulting nanostructure in a way that low energy surfaces are obtained. Only the concentrations of water and methanol were changed to modulate the polarity and to obtained different morphologies. When water was used as solvent it promoted the growth of hexagonal structures due to the formation of OH-1 ions in the solution [1,2]. The use of methanol with water resulted in hollow nanoprisms morphology likely due to the etching done by O^{-2} ions formed during the process [3]. While the use of organic solvent such as methanol/ethanol directed the growth of 1D nanorice morphology having high aspect ratio owing to its low polarity and high vapor pressure [4–6]. The grown nanoprisms and hollow nanoprisms possess a quite large size, which could be responsible for weak dye loading and resulted overall performance of DSSCs [7].

5.1 Structural analysis

X-ray powder diffractometry is a non-destructive technique to provide the information about the crystal structure, composition and the other physical properties of synthesized materials. XRD results for all the synthesized materials shows a hexagonal wurtzite structure of all the ZnO nanostructures was performed, the data were chosen in the range 20 - 80° of 2θ with the step-scan approach using 0.01° The synthesized nanostructures were confirmed with X-Ray diffraction analysis. X-Ray diffraction pattern of synthesized nanostructures (Fig.5.1) demonstrates the tetrahedral arrangement and wurtzite structure. Standard data of diffraction for synthesized ZnO nanostructures were assessed for comparison in figure 1 and it was found that peaks were in good agreement with those for ZnO, obtained from International Center of Diffraction Data Card (PDF No. 79-0208; P63mc(186), 80-0074; P63mc(186)) and 79-2205; P63mc(186)) for hollow hexagonal nanoprisms, nanoprisms and nanorice like structures respectively [2,8,9]. Pattern shows the dominant peak (101) and indicates

that grown structures are along both a and c axis. This pattern indicates that growth of nanostructures is dominant along (101) due to its lower surface energy [3,4]. XRD pattern of collected powder from hydrothermal synthesis process within the angular range of 2 theta 20-80, peaks clearly match with the hexagonal wurtzite crystal phase. The observed peaks at 2 thetas equal to 31.54, 34.221, 36.05, 47.236, 56.39, 62.65, 66.21, 67.71, 68.88, 72.42 and 76.96 indicate the reflection from the planes (001), (002), (101), (102), (110), (103), (200), (112), (201), (004) and (202) respectively. Except the peaks of wurtzite ZnO structure, no other peak is observed which indicate that no impurity is present in the final product of hydrothermal synthesis.

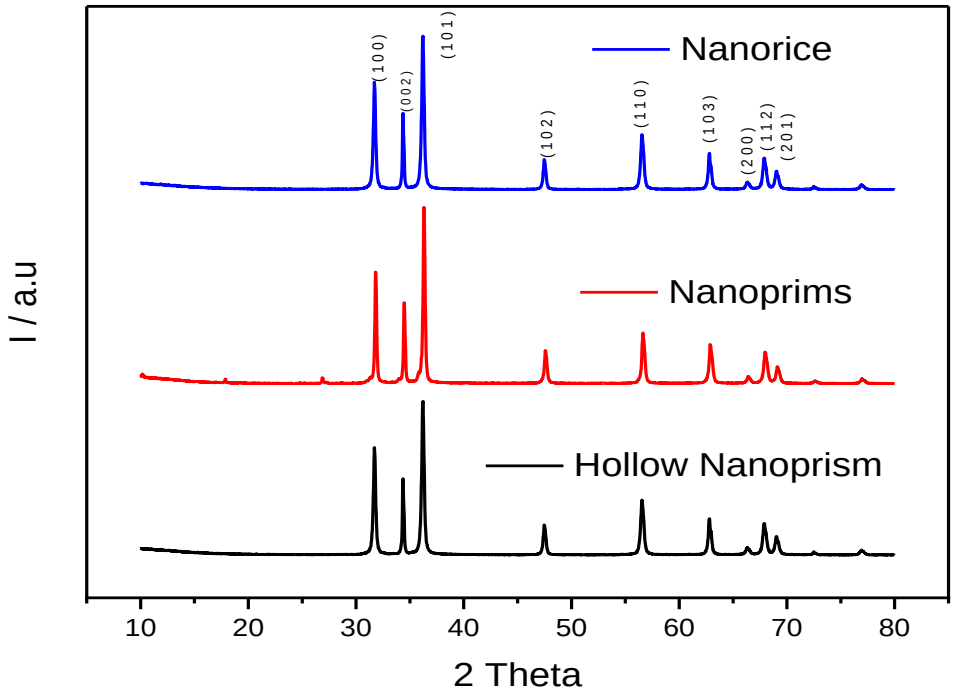

Fig. 5.1: XRD Pattern

5.2 Morphology and elemental analysis

Microstructure of ZnO nanostructures was analysed electron microscopy. SEM micrographs of all the nanostructures shown in Figure 2, a-c. It can clearly be seen that ZnO have different nanostructures i.e., hexagonal nano prisms, hollow nanoprisms and rice like morphologies. The size of nanoprisms and nonorice presented in figure 2a and 2c are almost equal. While the size of nanoprisms in figure 2b, is in the range of 140 nm to 322 nm with an average size of 226 nm was estimated. In figure 2a, it was noted that few prisms were broken ends and some are imploded indicate that their cores are hollow due to the presence of O^{-2} polar facets [3]. A wide size distribution is noted

with average size 386 nm for hollow hexagonal prisms. The larger size of hollow nanoprisms could be responsible for weak dye adsorption [2], [7] discussed in contact angle section. In contrast ZnO nanorice have size ranging from 112 nm to 200 nm. Nanorice like structures showed narrow size distribution almost equal in size with and an average size of 143 nm. Besides nanorice are agglomerated and stacked with each other in an irregular fashion. In addition, EDX analysis for elements reveal only the presence of Zn and O in the structural analysis.

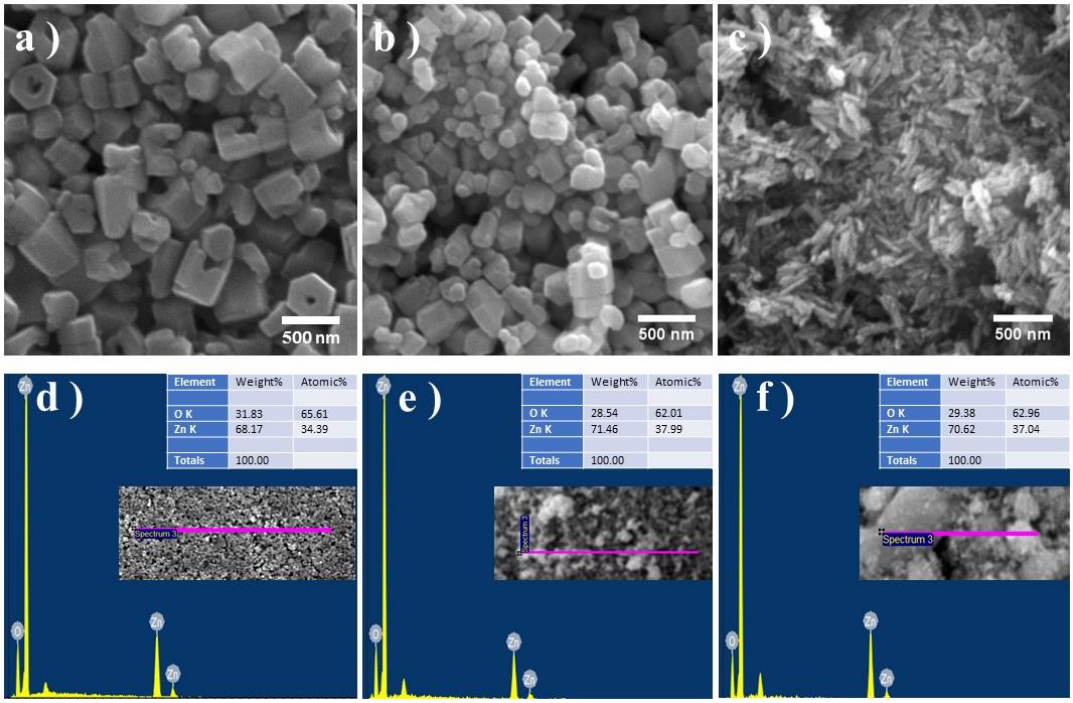

Fig. 5.2: SEM Images (a) Hollow nanoprism (b) Nanoprism (c) Nanorice; EDS analysis (d) Hollow nanoprism (e) Nanoprism (f) Nanorice

The exact percentages of elements of nanostructures are summarized in table 5.1.

Table 5 1: EDS analysis results

Element	Hollow nanoprism		Nanoprism		Nanorice	
	Weight%	Atomic%	Weight%	Atomic%	Weight%	Atomic%
O K	31.83	66.61	28.54	62.01	29.38	62.96
Zn K	68.17	34.39	71.46	37.99	70.62	37.04
Totals	100		100		100	

5.3 Optical properties

(Fig. 5.3, a-b) illustrate the behaviour of grown nanostructures on glass substrate for absorbance, which shows structures have high absorption edge in UV region while transparent in visible region as previously reported [5,6]. The dye adsorbed films increased the absorbance of material in visible region.

The diffused reflectance spectroscopy was performed for all three types of nanostructures with and without dye adsorption. The absorbance plots were drawn using the Kubelka-Munk function [14] to show the change in absorbance after dye adsorption and for band gap analysis.

$$[\mathbf{F(R)h\upsilon}] = \mathbf{A(h\upsilon - Eg)^n} \qquad \textbf{(5.1)}$$

$$\boldsymbol{F(R)} = \frac{\boldsymbol{(1-R)^2}}{\boldsymbol{2R}} \qquad \textbf{(5.2)}$$

Where, h is Plank constant

A is absorbance,

R is reflectance

Eg is the band gap of material and n is ½ and 2 for indirect and direct bandgap semiconductor materials respectively.

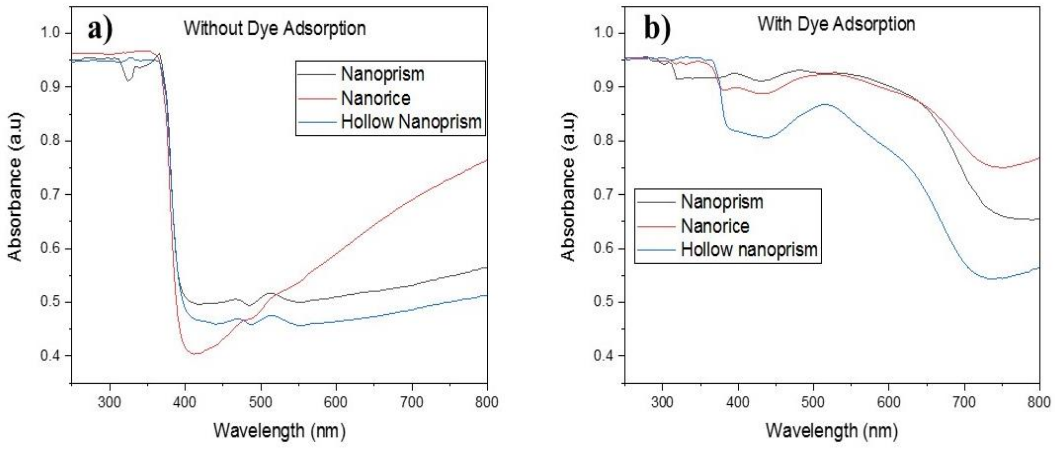

Fig. 5.3: Absorption Spectra of photoanodes (a) Without Dye adsorption (b) With dye adsorption

Bandgap for grown nanostructures were calculated using the Tauc plots as shown in figure 4. Band gap was deduced using the plot 3.23 eV, 3.2 eV and 3.24 eV for hollow

nanoprisms, nanoprisms and nanorice like structures respectively. the slight change in band gap is due to change in diameter of nanostructures.

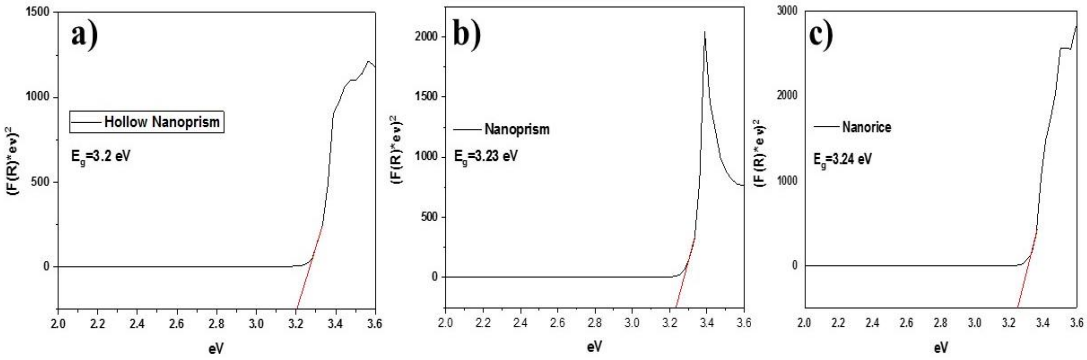

Fig. 5.4: Band gap analysis (a) Hollow nanoprism (b) Nanoprism (c) Nanorice

5.4 Surface area analysis

Nitrogen adsorption/ desorption isotherm was obtained after performing BET analysis for surface area, pore size and pore volume distribution study. The particulate properties of grown samples, such as surface area, pore size and pore volume are summarized in table 5.2.

Table 5. 2: BET analysis by BJH area-volume summary of Hollow nanoprisms, Nanoprisms and Nanorice

Sample ID	Surface area (m^2/g)	Pore Volume (cc/g)	Pore Size (Å)
Nanorice	$2.272x10^{1}$	$1.152x10^{-1}$	$8.368x10^{1}$
Nanoprism	$1.058x10^{1}$	$7.388x10^{-3}$	$1.819x10^{1}$
Hollow Nanoprism	$5.896x10^{0}$	$5.237x10^{-3}$	$2.023x10^{1}$

The BET surface area was 1.474, 2.645 and 22.72, respectively for hollow nanoprism, nanoprism and nanorice like structures. The high surface area of nanorice might be due the small size observed in morphological analysis could be the responsible for improved dye loading [15]. The high surface area and pore size are beneficial for dye sensitized solar cells as this help for more dye loading [16] and improve the permeation of the electrolyte [17,18]. The assumption is based on literature evidence; in fact, multiple

researchers have shown that even a little change in dye loading effect the performance of DSSCs such as V_{oc} for ZnO [19] as well as TiO_2 [18]. Adsorption and desorption isotherm of grown structures are shown in fig. 5. The area under the hysteresis loop is decreased, indicating the increased pore size.

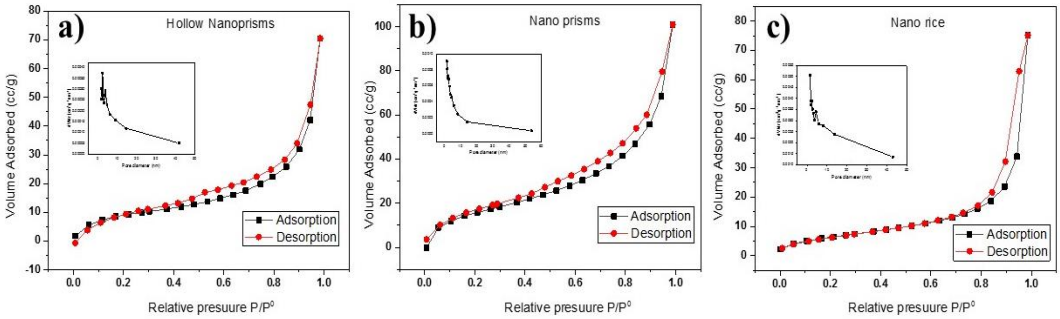

Fig. 5.5: N2 adsorption and desorption isotherms (a) Hollow nanoprsim (b) Nanoprism (c) Nanorice

5.5 Electrical Properties

Electrical properties of thin films based on grown nanostructures were analysed by Hall effect measurement. Thickness of each sample before conducting hall effect measurement was identified by using profilometer (P.10 KLA-Tencor Profiler). Table 1 illustrate the electrical properties of grown structures like bulk concentration, mobility and conductivity. It is found from results that nanorice like structure being a 1-d structures shown more conductivity values due to fast electron injection [20] which help to improve the conversion efficiency of nanorice based DSSCs [21]. While in comparison nanoprism and hollow nanoprism has shown lower conductivity values which contribute to lower conversion efficiency for hollow nanoprism based DSSCs.

Table 5.3: Hall effect measurements for conductivity values of Hollow nanoprsims, Nanoprsims and Nanorice

Sample ID	Bulk concentration (/cm^3)	Mobility (cm^2/Vs)	Conductivity (1/Ω cm)
Nanorice	-1.984x10^{13}	6.539x10^{0}	2.079x10^{-5}
Nanoprism	-1.738x10^{13}	6.673x10^{0}	1.858x10^{-5}
Hollow Nanoprism	-4.203x10^{12}	4.278x10^{0}	2.881x10^{-6}

Typical current-voltage curves measured for fabricated DSSCs based on grown nanostructures and a reference cell based on TiO_2 using N719 dye. The obtained current density-voltage (J-V) curves are reported in figure 5.6 and electrical parameters such as; open circuit voltage (Voc), short circuit current (Isc), maximum voltage (Vmp), maximum current (Imp), fill factor (FF) and efficiency (ɳ) obtained from I-V measurements against each grown structure are listed in table 3.

The open circuit voltage value for all grown nanostructures is almost same, the fact is that Voc is solely determined by the potential difference between the fermi band edge and the redox couple potential (Iodolyte in our case) [22], and that it is unaffected by the series resistance because the current flow is zero when the Voc is measured. While Voc for TiO_2 is high in comparison to ZnO which is already reported in previous study [23].

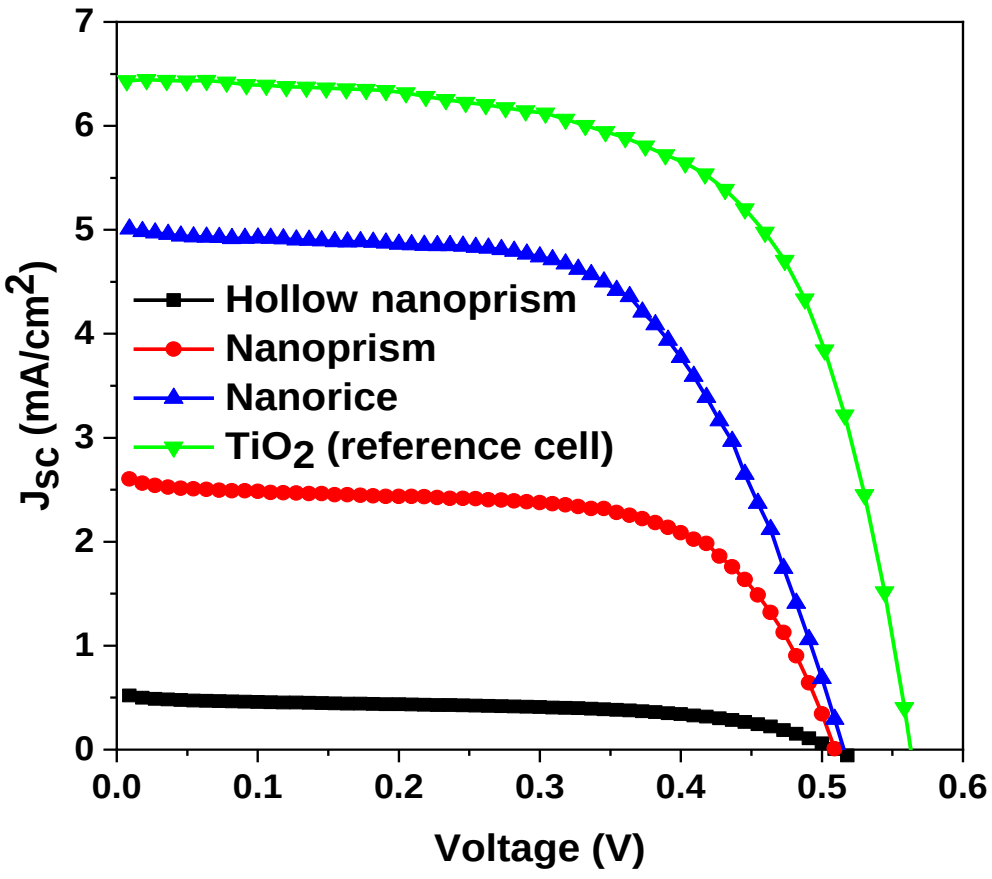

Fig. 5.6: J-V Curves of homegrown nanostructure based DSSCs

The main difference which observed is short circuit current, that is attributed due to better dye adsorption on nanorice like structures based photoanodes owing to high surface area and lower contact angle in comparison to nanoprisms and hollow

nanoprisms. Enhanced dye loading help to harvest more solar light, leading to higher short circuit current [24].

The decrease in series resistance for nanorice like structures shown higher fill factor value as compared to hollow nanoprism. Interface between redox couple and ZnO nanorice based photoanode results in low series resistance and efficient dye regeneration [25] possibly due to smaller diameter of nanostructures, more thickness and homogeneity of thin films over the substrate surface. The photoconversion efficiency reached 0.18%, 1.11% and 2.11% for hollow nanoprisms, nanoprisms and rice like nanostructures respectively. A TiO_2 based reference DSSC using N719 dye was also tested which has shown the conversion efficiency of 3.09%.

The photovoltaic parameters; open circuit voltage (Voc), short circuit current (Isc), maximum voltage (Vmp), maximum current (Imp), fill factor (FF) and efficiency (η) obtained from I-V measurements against each grown structure have been listed in table 5.4.

Table 5.4: Photovoltaic parameters of all fabricated DSSCs.

Sample ID	Vmp (V)	Imp (mA/cm^2)	Voc (V)	Isc (mA/cm^2)	FF	η (%)
Nanorice	0.363655	4.357487	0.518159	5.88745	0.519439	2.112826
Nanoprism	0.409139	2.058672	0.563647	2.787836	0.536024	1.123044
Hollow Nanoprism	0.381812	0.359714	0.509067	0.644291	0.418745	0.183124

The external quantum efficiency (EQE) of DSSCs is performed and shown in figure 5.7. In the wavelength range of 400 to 600nm devices performed efficiently with the highest EQE of 52.9% for nanorice like structures at 520 nm. Similar behaviour was shown by nanoprisms and hollow nanoprisms but the highest value of EQE is lower than nanorice like structures. The active wavelength region for EQE of DSSCs shown in result is in a good arrangement with active UV-Vis region of dye adsorbed photoanodes.

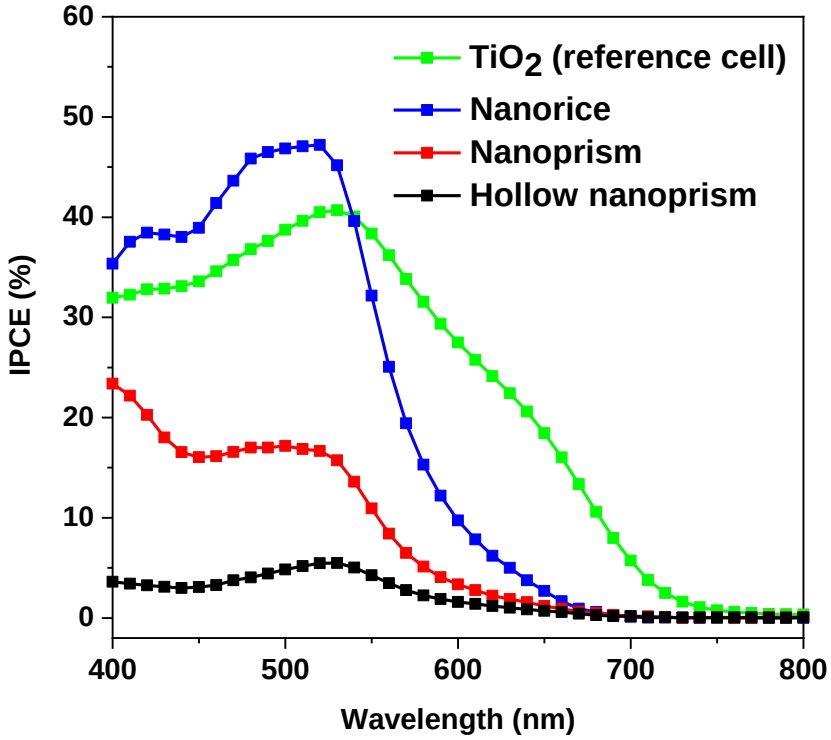

Fig. 5.7: External quantum efficiency curves for Hollow nanoprism, Nanoprisms and Nanorice

Summary

This chapter contains the results of method employed for the characterization discussed in above chapter and their relevant discussion of analysis performed on the results of characterization techniques for our synthesized materials. All the results and facts from previous studies are justified to understand the morphology and performance. All the results show in good agreement with the final efficiency value achieved.

Reference

[1] X. G. Han *et al.*, "Controlling morphologies and tuning the related properties of nano/microstructured ZnO crystallites, vol. 113, no. 2, pp. 584–589, 2009.

[2] M. Ramzan Parra, P. Pandey, H. Siddiqui, V. Sudhakar, K. Krishnamoorthy, and F. Z. Haque, "Evolution of ZnO nanostructures as hexagonal disk: Implementation as photoanode material and efficiency enhancement in Al: ZnO based dye sensitized solar cells," vol. 470, pp. 1130–1138, 2019.

[3] M. Ramzan Parra, P. Pandey, H. Siddiqui, V. Sudhakar, K. Krishnamoorthy, and F. Z. Haque, "Evolution of ZnO nanostructures as hexagonal disk: Implementation as photoanode material and efficiency enhancement in Al: ZnO based dye sensitized solar cells, vol. 470, pp. 1130–1138, 2019.

[4] B. Sikora *et al.*, "The growth kinetics of colloidal ZnO nanoparticles in alcohols, vol. 61, no. 1, pp. 197–205, 2012.

[5] F. Ahmed, N. Arshi, M. S. Anwar, R. Danish, and B. H. Koo, "Morphological evolution of ZnO nanostructures and their aspect ratio-induced enhancement in photocatalytic properties, vol. 4, no. 55, pp. 29249–29263, 2014.

[6] S. Thakur and S. K. Mandal, "Investigating the formation of diverse ZnO nanostructures based on solvent, temperature, and pH as adjustable parameters, vol. 2, no. 1, pp. 511–524, 2021.

[7] Y. He, J. Hu, and Y. Xie, "High-efficiency dye-sensitized solar cells of up to 8.03% by air plasma treatment of ZnO nanostructures, vol. 51, no. 90, pp. 16229–16232, 2015.

[8] L. Bahadur and S. Kushwaha, "Structural and optical properties of tripod-like ZnO thin film and its application in dye-sensitized solar cell, vol. 17, no. 7, pp. 2001–2008, 2013.

[9] Q. Li, V. Kumar, Y. Li, H. Zhang, T. J. Marks, and R. P. H. Chang, "Fabrication of ZnO nanorods and nanotubes in aqueous solutions, vol. 17, no. 5, pp. 1001–1006, 2005.

[10] S. Liang and X. Bi, "Structure, conductivity, and transparency of Ga-doped ZnO thin films arising from thickness contributions, vol. 104, no. 11, p. 113533,

2008.

[11] J. Lv, J. Zhu, K. Huang, F. Meng, X. Song, and Z. Sun, "Tunable surface wettability of ZnO nanorods prepared by two-step method, vol. 257, no. 17, pp. 7534–7538, 2011.

[12] M. C. Kao, H. Z. Chen, S. L. Young, C. C. Lin, and C. Y. Kung, "Structure and photovoltaic properties of Zno nanowire for dye-sensitized solar cells, vol. 7, no. 1, pp. 1–6, 2012.

[13] R. Haarindraprasad *et al.*, "Low temperature annealed zinc oxide nanostructured thin film-based transducers: Characterization for sensing applications, vol. 10, no. 7, p. e0132755, 2015.

[14] S. S. Abdullahi, S. Güner, Y. Koseoglu, I. Murtala, B. I. Adamu, and M. I. Abdulhamid, "Sımpl e Method For The Determ ınatıon o f Band Gap of a Nanopowdered Sample Usıng Kubelka Munk Theory, vol. 35, pp. 241–246, 2016.

[15] H. Sayahi, K. Aghapoor, F. Mohsenzadeh, M. Mohebi Morad, and H. R. Darabi, "TiO_2 nanorods integrated with titania nanoparticles: Large specific surface area 1D nanostructures for improved efficiency of dye-sensitized solar cells (DSSCs), vol. 215, pp. 311–320, 2021.

[16] Q. Zhang, S. Hou, and C. Li, "Titanium dioxide-coated zinc oxide nanorods as an efficient photoelectrode in dye-sensitized solar cells, vol. 10, no. 8, pp. 1–9, 2020.

[17] Z. S. Wang, H. Kawauchi, T. Kashima, and H. Arakawa, "Significant influence of TiO_2 photoelectrode morphology on the energy conversion efficiency of N719 dye-sensitized solar cell, vol. 248, no. 13–14. pp. 1381–1389, 2004.

[18] E. Dell'Orto, L. Raimondo, A. Sassella, and A. Abbotto, "Dye-sensitized solar cells: Spectroscopic evaluation of dye loading on TiO_2, vol. 22, no. 22, pp. 11364–11369, 2012.

[19] S. B. Ambade *et al.*, "Contact angle measurement: A preliminary diagnostic method for evaluating the performance of ZnO platelet-based dye-sensitized solar cells, vol. 61, no. 1, pp. 12–15, 2009.

[20] T. P. Yendrapati, A. Gautam, S. Bojja, and U. Pal, “Formation of ZnO@CuS nanorods for efficient photocatalytic hydrogen generation, vol. 196, pp. 540–548, 2020.

[21] K. Virkki, E. Tervola, M. Ince, T. Torres, and N. V. Tkachenko, “Comparison of electron injection and recombination on TiO_2 nanoparticles and ZnO nanorods photosensitized by phthalocyanine, vol. 5, no. 7, 2018.

[22] J. Chang *et al.*, “ZnO nanocones with high-index {10$\bar{1}$1} facets for enhanced energy conversion efficiency of dye-sensitized solar cells, vol. 117, no. 27, pp. 13836–13844, 2013.

[23] N. Shahzad *et al.*, “Comparison of hemi-squaraine sensitized TiO_2 and ZnO photoanodes for DSSC applications, vol. 117, no. 44, pp. 22778–22783, 2013.

[24] W. C. Chang, C. H. Lee, W. C. Yu, and C. M. Lin, “Optimization of dye adsorption time and film thickness for efficient ZnO dye-sensitized solar cells with high at-rest stability, vol. 7, no. 1, pp. 1–10, 2012.

[25] S. Rani, P. Suri, and R. M. Mehra, “Mechanism of charge recombination and IPCE in ZnO dye-sensitized solar cells having I^-/I_3^- and Br^-/Br_3^- redox couple, vol. 19, no. 2, pp. 180–186, 2011.

Chapter 6

Conclusion and Recommendations

6.1 Conclusions

ZnO nanostructures were successfully synthesized by changing solvating conditions and deposited on FTO substrate by employing drop casting technique. The structure, morphology, optical and electrical properties were thoroughly investigated. The findings revealed that the grown nanostructures are in a good agreement with ZnO wurtzite phase. The growth of nanoprisms along c-axis attributed to the presence of OH^{-1} ion in aqueous solution while the formation of nanorice-like structures in organic solutions can be linked to the dissolution of the c-axis polar surface (0001), which has a low chemical stability. Etching done by O^{-2} ions formed in dual solvent resulted in hollow nanoprism. Hollow nanoprism possess larger size, lower specific area and an increased water contact angle which proved that the surface is more hydrophobic in comparison to nanoprism and nanorice like structures. All these factors attribute to low dye impregnation which is evident from lower optical absorbance. Finally, DSSCs were fabricated using nanostructures based photoanodes for IV measurements, the results shown the highest photoconversion efficiency of 2.11% for nanorice like structures followed by nanoprism (1.11%) and hollow nanoprism (0.18%).

6.2 Recommendations

Various electrolytes, dyes and photoanode materials have been emerging in the result of continuous development of dye sensitized solar cells. Photoanode with improved both electrical and optical properties is yet to be considered for future work to make DSSCs economically attractive. Following are the few recommended future works.

- Improvements to the aqueous solution method for improved aspect ratio management and better reactant usage
- Development of new dyes which show the more conversion efficiencies for ZnO based DSSCs.
- Multiple depositions of different nanostructures to increase surface area and electron injection properties.

- Investigation of growth mechanism by using more than one solvent for zinc acetate as well as for basic solution.
- Use of rust-free copper connections, pure solvent and new dye can enhance the performance of dye sensitized solar cells.

Journal Paper

Effect of ZnO nanostructures on the performance of dye sensitized solar cells

Ahad Hussain Javed[a,b], *Nadia Shahzad[a], M. Abdullah Khan[b], Muniba Ayub[a], Naseem Iqbal[a], Muhammad Hassan[a], Naveed Hussain[a], Muhammad Imran Rameel[a,b], Muhammad Imran Shahzad[c]

[a]*U.S.-Pakistan Centre for Advanced Studies in Energy (USPCAS-E), National University of Sciences & Technology (NUST), H-12 Sector (44000) Islamabad, Pakistan*
[b]*Renewable Energy Advancement Laboratory (REAL), Department of Environmental Sciences, Quaid-i-Azam University Islamabad*
[c]*Nanosciences and Technology Department (NS&TD), National Centre for Physics (NCP), 44000 Islamabad, Pakistan*

Graphical Abstract:

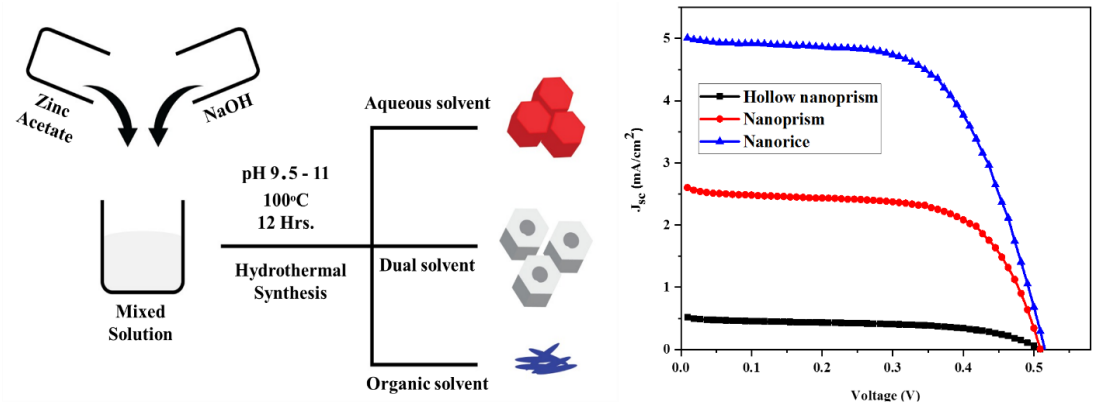

Abstract

Development of cost effective and easily scalable energy systems for harvesting renewable solar energy is attractive proposal for future. This work presents facile synthesis of ZnO nanostructures with different morphologies simply providing different solvating conditions in a hydrothermal process, for their subsequent use in dye sensitized solar cell (DSSC) device. ZnO nanoprisms were obtained in aqueous solution where addition of methanol/ethanol resulted in formation of hollow nanoprims while methanol in alkaline solution yield ZnO nanorice morphology. The obtained nanostructures were characterized for structural, morphological, elemental, optical and surface area analysis. Then devices were fabricated using the grown nanostructure and tested their response under 1 sun conditions for dye sensitized solar cells with N719 dye loading. Among the different nanostructure morphologies, ZnO nonorice showed superior performance reaching the maximum conversion efficiency. We attribute this to the large surface area, better conductivity, and enhanced dye adsorption of nanorice in comparison to the other synthesized ZnO nanostructures.

Keywords: *ZnO, Hexagonal nanoprsim, Nanorice, Hydrothermal, DSSCs*

The Development of Highly Fluorescent Hemicyanine and Dicyanoisophorone Dyes for Applications in Dye-Sensitized Solar Cells

Ghulam Shabir[a], Sama Arooj[a], Ahad Hussain Javed[b], Aamer Saeed[a*], Nadia Shahzad[b], Naseem Iqbal[b], Erum Jabeen[c]

[a] *Department of Chemistry, Quaid-I-Azam University, Islamabad 45320, Pakistan.*

[b] *U.S.-Pakistan Centre for Advanced Studies in Energy (USPCAS-E), National University of Sciences & Technology (NUST), H-12 Sector (44000) Islamabad, Pakistan.*

[c] *Department of Chemistry, Allama Iqbal Open University, H-8, Islamabad 44000, Pakistan.*

Graphical Abstract

The Development of Highly Fluorescent Hemicyanine and Dicyanoisophorone Dyes for Applications in Dye-Sensitized Solar Cells

Ghulam Shabir, Sama Arooj, Ahad Hussain, Aamer Saeed , Nadia Shahzad, Naseem Iqbal, Erum Jabeen

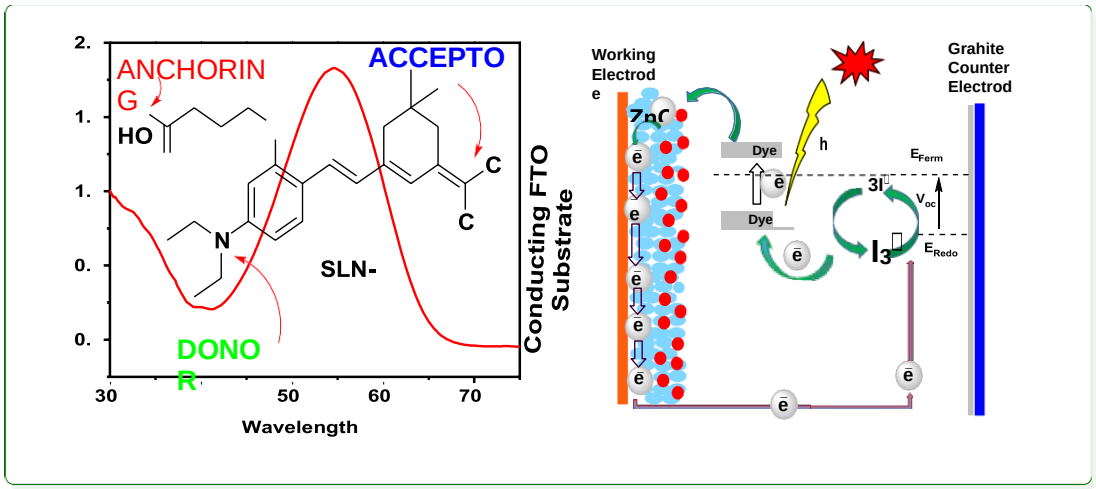

Abstract

Ruthenium-based metal complex dyes have been employed extensively in dye-sensitized solar cells (DSSCs) as photosensitizers, but the cost and toxicity of metal complexes have promoted the development of metal-free organic dyes. The present investigation deals with the synthesis of hemicyanine and Dicyanoisophorone (DCI) based dyes adopting the D-π-A strategy, and their application on sensitization of nano-crystalline ZnO electrodes by appending the carboxyl (COOH) anchoring group as a pendant on the primary skeleton of dyes. Dyes have been characterized by UV, FTIR, and NMR spectroscopic studies. Absorption maxima (λmax) were found in the region 416-551nm while emission wavelength (λem) was blazed in the range 575- 685nm. The photoconversion efficiency reached 0.13%, 0.026%, and 0.085% with mask for dye SLN-01, SLN-02 and SLN-03 respectively on ZnO-based DSSCs. Cyclic voltammetry and DFT calculations were used to estimate redox potential and bandgap energies of dyes.

Keywords: Photosensitizers; Hemicyanine; Isophorone; D-π-A strategy; Nano-crystalline ZnO; Photoconversion Efficiency.